

Bi-allelic *ACBD6* variants lead to a neurodevelopmental syndrome with progressive and complex movement disorders

Rauan Kaiyrzhanov,^{1,†} Aboufazel Rad,^{2,3,†} Sheng-Jia Lin,^{4,†} Aida Bertoli-Avella,^{5,†} Wouter W. Kallemeijn,^{6,7,†} Annie Godwin,^{8,†} Maha S. Zaki,⁹ Kevin Huang,⁴ Tracy Lau,¹ Cassidy Petree,⁴ Stephanie Efthymiou,¹ Ehsan Ghayoor Karimiani,^{10,11} Maja Hempel,^{12,13} Elizabeth A. Normand,¹⁴ Sabine Rudnik-Schöneborn,¹⁵ Ulrich A. Schatz,^{15,16} Marc P. Baggelaar,^{6,17} Muhammad Ilyas,^{18,19} Tipu Sultan,²⁰ Javeria Raza Alvi,²⁰ Manizha Ganieva,²¹ Ben Fowler,²² Ruxandra Aanicai,⁵ Gulsen Akay Tayfun,²³ Abdulaziz Al Saman,²⁴ Abdulrahman Alswaid,²⁵ Nafise Amiri,²⁶ Nilufar Asilova,²¹ Vorasuk Shotelersuk,²⁷ Patra Yeetong,²⁸ Matloob Azam,²⁹ Meisam Babaei,³⁰ Gholamreza Bahrami Monajemi,³¹ Pouria Mohammadi,^{32,33} Saeed Samie,³¹ Selina Husna Banu,³⁴ Jorge Pinto Basto,⁵ Fanny Kortüm,¹² Mislen Bauer,³⁵ Peter Bauer,⁵ Christian Beetz,⁵ Masoud Garshasbi,³³ Awatif Hameed Issa,³⁶ Wafaa Eyaid,³⁷ Hind Ahmed,³⁷ Narges Hashemi,³⁸ Kazem Hassanpour,³⁹ Isabella Herman,^{40,41,42,43} Sherozjon Ibrohimov,²¹ Ban A. Abdul-Majeed,⁴⁴ Maria Imdad,⁴⁵ Maksudjon Isrofilov,²¹ Qassem Kaiyal,⁴⁶ Suliman Khan,⁵ Brian Kirmse,⁴⁷ Janet Koster,⁴⁸ Charles Marques Lourenço,⁴⁹ Tadahiro Mitani,⁴¹ Oana Moldovan,⁵⁰ David Murphy,⁵¹ Maryam Najafi,^{52,53} Davut Pehlivan,^{40,41} Maria Eugenia Rocha,⁵ Vincenzo Salpietro,¹ Miriam Schmidts,^{52,53,54} Adel Shalata,^{55,56} Mohammad Mahroum,⁵⁴ Jawabreh Kassem Talbeya,^{55,57} Robert W. Taylor,^{58,59} Dayana Vazquez,³⁵ Annalisa Vetro,⁶⁰ Hans R. Waterham,⁴⁸ Mashaya Zaman,³⁴ Tina A. Schrader,⁶¹ Wendy K. Chung,^{62,63} Renzo Guerrini,^{60,64} James R. Lupski,^{41,42,65} Joseph Gleeson,^{66,67} Mohnish Suri,⁶⁸ Yalda Jamshidi,^{10,69} Kailash P. Bhatia,⁵¹ Barbara Vona,^{3,70,71} Michael Schrader,⁶¹ Mariasavina Severino,⁷² Matthew Guille,^{8,‡} Edward W. Tate,^{6,7,‡} Gaurav K. Varshney,^{4,‡} Henry Houlden^{1,‡} and Reza Maroofian^{1,‡}

^{†,‡}These authors contributed equally to this work.

1 Abstract

2 The acyl-CoA-binding domain-containing protein 6 (ACBD6) is ubiquitously expressed, plays a
3 role in the acylation of lipids and proteins, and regulates the *N*-myristoylation of proteins via *N*-
4 myristoyltransferase enzymes (NMTs). However, its precise function in cells is still unclear, as is
5 the consequence of *ACBD6* defects on human pathophysiology. Utilizing exome sequencing and
6 extensive international data sharing efforts, we identified 45 affected individuals from 28
7 unrelated families (consanguinity 93%) with bi-allelic pathogenic, predominantly loss-of-
8 function (18/20) variants in *ACBD6*. We generated zebrafish and *Xenopus tropicalis acbd6*
9 knockouts by CRISPR/Cas9 and characterized the role of *ACBD6* on protein *N*-myristoylation
10 with YnMyr chemical proteomics in the model organisms and human cells, with the latter also
11 being subjected further to ACBD6 peroxisomal localization studies. The affected individuals (23
12 males and 22 females), with ages ranging from 1 to 50 years old, typically present with a
13 complex and progressive disease involving moderate-to-severe global developmental
14 delay/intellectual disability (100%) with significant expressive language impairment (98%),
15 movement disorders (97%), facial dysmorphism (95%), and mild cerebellar ataxia (85%)
16 associated with gait impairment (94%), limb spasticity/hypertonia (76%), oculomotor (71%) and
17 behavioural abnormalities (65%), overweight (59%), microcephaly (39%) and epilepsy (33%).
18 The most conspicuous and common movement disorder was dystonia (94%), frequently leading
19 to early-onset progressive postural deformities (97%), limb dystonia (55%), and cervical
20 dystonia (31%). A jerky tremor in the upper limbs (63%), a mild head tremor (59%),
21 parkinsonism/hypokinesia developing with advancing age (32%), and simple motor and vocal
22 tics were among other frequent movement disorders. Midline brain malformations including
23 corpus callosum abnormalities (70%), hypoplasia/agenesis of the anterior commissure (66%),
24 short midbrain and small inferior cerebellar vermis (38% each), as well as hypertrophy of the
25 clava (24%) were common neuroimaging findings. *acbd6*-deficient zebrafish and *Xenopus*
26 models effectively recapitulated many clinical phenotypes reported in patients including
27 movement disorders, progressive neuromotor impairment, seizures, microcephaly, craniofacial
28 dysmorphism, and midbrain defects accompanied by developmental delay with increased
29 mortality over time. Unlike ACBD5, ACBD6 did not show a peroxisomal localisation and
30 ACBD6-deficiency was not associated with altered peroxisomal parameters in patient

1 fibroblasts. Significant differences in YnMyr-labelling were observed for 68 co- and 18 post-
2 translationally *N*-myristoylated proteins in patient-derived fibroblasts. *N*-Myristoylation was
3 similarly affected in *acbd6*-deficient zebrafish and *Xenopus tropicalis* models, including Fus,
4 Marcks, and Chchd-related proteins implicated in neurological diseases. The present study
5 provides evidence that bi-allelic pathogenic variants in *ACBD6* lead to a distinct
6 neurodevelopmental syndrome accompanied by complex and progressive cognitive and
7 movement disorders.

8

9 **Author affiliations:**

10 1 Department of Neuromuscular diseases, UCL Institute of Neurology, WC1N 3BG, London,
11 UK

12 2 Cellular and Molecular Research Center, Sabzevar University of Medical Sciences, Sabzevar
13 009851, Iran

14 3 Tübingen Hearing Research Centre, Department of Otolaryngology, Head and Neck Surgery,
15 Eberhard Karls University, 72076, Tübingen, Germany

16 4 Genes & Human Disease Research Program, Oklahoma Medical Research Foundation,
17 Oklahoma City, OK, 73104, USA

18 5 CENTOGENE GmbH, 18055, Rostock, Germany

19 6 Department of Chemistry, Imperial College London, Molecular Sciences Research Hub,
20 London, W12 0BZ, UK

21 7 The Francis Crick Institute, London, NW1 1AT, UK

22 8 European *Xenopus* Resource Centre - XenMD, School of Biological Sciences, University of
23 Portsmouth, PO1 2DT, UK.

24 9 Clinical Genetics Department, Human Genetics and Genome Research Institute, National
25 Research Centre, 12622, Cairo, Egypt

26 10 Genetics Research Centre, Molecular and Clinical Sciences Institute, St George's University
27 of London, SW17 0RE, London, UK

- 1 11 Department of Medical Genetics, Next Generation Genetic Polyclinic, Mashhad, Iran
- 2 12 Institute of Human Genetics, University Medical Center Hamburg-Eppendorf, 20246,
3 Hamburg, Germany
- 4 13 Institute of Human Genetics, University Hospital Heidelberg, Heidelberg, 69120, Germany
- 5 14 GeneDx, Gaithersburg, 20877, Maryland, USA
- 6 15 Institute of Human Genetics, Medical University Innsbruck, 6020, Austria
- 7 16 Institute of Human Genetics, Technical University of Munich, 81675, Germany
- 8 17 Utrecht University, Biomolecular Mass Spectrometry & Proteomics Group, 3584 CH Utrecht,
9 The Netherlands
- 10 18 Department of BioEngineering, University of Engineering and Applied Sciences, 19130,
11 Swat, Pakistan
- 12 19 Centre for Omic Sciences, Islamia College University, 25000, Peshawar, Pakistan
- 13 20 Department of Pediatric Neurology, Institute of Child Health, Children Hospital, Lahore,
14 Pakistan
- 15 21 Department of Neurology, Avicenna Tajik State Medical University, 734063, Dushanbe,
16 Tajikistan
- 17 22 Imaging Core, Oklahoma Medical Research Foundation, Oklahoma City, OK, 73104, USA
- 18 23 Department of Pediatric Genetics, Marmara University Medical School, 34722, Istanbul,
19 Turkey
- 20 24 Pediatric Neurology Department, National Neuroscience Institute, King Fahad Medical City,
21 49046, Riyadh, Saudi Arabia
- 22 25 King Saud Bin Abdulaziz University For Health Sciences, Department of Pediatrics, King
23 Abdullah Specialized Children's Hospital, Riyadh, Saudi Arabia
- 24 26 International Collaboration on Repair Discoveries (ICORD), University of British Columbia,
25 V5Z 1M9, Vancouver, Canada
- 26 27 Center of Excellence for Medical Genomics, Department of Pediatrics, King Chulalongkorn
27 Memorial Hospital, Faculty of Medicine, Chulalongkorn University, Bangkok 10330, Thailand

- 1 28 Division of Human Genetics, Department of Botany, Faculty of Science, Chulalongkorn
2 University, Bangkok 10330, Thailand
- 3 29 Pediatrics and Child Neurology, Wah Medical College, 47000, Wah Cantt, Pakistan
- 4 30 Department of Pediatrics, North Khorasan University of Medical Sciences, Bojnurd, Iran
- 5 31 Pars Advanced and Minimally Invasive Medical Manners Research Center, Pars Hospital,
6 1415944911, Tehran, Iran
- 7 32 Children's Medical Center, Pediatrics Center of Excellence, Ataxia Clinic, Tehran University
8 of Medical Sciences, Tehran, Iran
- 9 33 Faculty of Medical Sciences, Department of Medical Genetics, Tarbiat Modares University,
10 Tehran, Iran
- 11 34 Department of Paediatric Neurology and Development, Dr. M.R. Khan Shishu (Children)
12 Hospital and Institute of Child health, Mirpur, Dhaka- 1216, Bangladesh
- 13 35 Division of Clinical Genetics and Metabolism, Nicklas Children's Hospital, Miami, Florida,
14 FL 33155, USA
- 15 36 University of Basrah, 61004, Basrah, Iraq
- 16 37 Department of genetics and precision medicine, King Abdullah International Medical
17 Research Centre, King Saud bin Abdulaziz University for Health Science, King Abdulaziz
18 Medical City, Ministry of National Guard-Health Affairs (NGHA), Riyadh, Saudi Arabia
- 19 38 Department of Pediatrics, school of Medicine, Mashhad University of Medical Sciences,
20 13131 – 99137, Mashhad, Iran
- 21 39 Non-Communicable Diseases Research Center, Sabzevar University of Medical Sciences,
22 319, Sabzevar, Iran
- 23 40 Section of Pediatric Neurology and Developmental Neuroscience, Department of Pediatrics,
24 Baylor College of Medicine, 68010, Houston, TX, USA
- 25 41 Department of Molecular and Human Genetics, Baylor College of Medicine, TX 77030
26 Houston, TX, USA
- 27 42 Texas Children's Hospital, Houston, TX 77030, TX, USA

1 43 Pediatric Neurology, Neurogenetics and Rare Diseases, Boys Town National Research
2 Hospital, 68131, Boys Town, NE, USA

3 44 Molecular Pathology and Genetics, The Pioneer Molecular Pathology Lab, Baghdad, Iraq

4 45 Centre for Human Genetics, Hazara University, 21300, Mansehra, Pakistan

5 46 Department of Pediatric Neurology, Clalit Health Care, 2510500, Haifa, Israel

6 47 University of Mississippi Medical Center, 2500, MS 39216, USA

7 48 Laboratory Genetic Metabolic Diseases, Amsterdam University Medical Centers location
8 AMC, 1100 DD, Amsterdam, The Netherlands

9 49 Faculdade de Medicina, Centro Universitario Estácio de Ribeirão Preto, Ribeirão Preto,
10 14096-160, São Paulo, Brazil

11 50 Serviço de Genética Médica, Departamento de Pediatria, Hospital de Santa Maria, Centro
12 Hospitalar Universitário de Lisboa Norte, 1649-035, Lisboa, Portugal

13 51 Department of Clinical and Movement Neurosciences, UCL Queen Square Institute of
14 Neurology, University College London, WC1N 3BG, London, UK

15 52 Pediatrics Genetics Division, Center for Pediatrics and Adolescent Medicine, Faculty of
16 Medicine, Freiburg University, 79106 Freiburg, Germany

17 53 Genome Research Divisio, Human Genetics Department, Radboud University Medical
18 Center, 6500 HB, Nijmegen, The Netherlands

19 54 CIBSS-Centre for Integrative Biological Signalling Studies, University of Freiburg, Freiburg,
20 Germany

21 55 Pediatrics and Medical Genetics, the Simon Winter Institute for Human Genetics, Bnai Zion
22 Medical Center, 31048, Haifa, Israel

23 56 Bruce Rappaport Faculty of Medicine, the Technion institution of Technology, 3200003,
24 Haifa, Israel

25 57 Department of Radiology, The Bnai Zion Medical Center, Haifa, Israel

26 58 Wellcome Centre for Mitochondrial Research, Translational and Clinical Research Institute,
27 Faculty of Medical Sciences, Newcastle University, Newcastle upon Tyne, NE2 4HH, UK

1 59 NHS Highly Specialised Service for Rare Mitochondrial Disorders, Newcastle upon Tyne
2 Hospitals NHS Foundation Trust, Newcastle upon Tyne, NE1 4LP, UK

3 60 Neuroscience Department, Meyer Children's Hospital IRCCS, 50139 Florence, Italy

4 61 Department of Biosciences, University of Exeter, EX4 4QD, Exeter, UK

5 62 Department of Pediatrics, Columbia University Irving Medical Center,
6 New York, NY 10032, USA

7 63 Department of Medicine, Columbia University Irving Medical Center, New York, NY 10032,
8 USA

9 64 University of Florence, 50139 Florence, Italy

10 65 Human Genome Sequencing Center, Baylor College of Medicine, Houston, Texas, 77030,
11 USA

12 66 Department of Neurosciences, University of California, San Diego, La Jolla, CA, 92093,
13 USA

14 67 Rady Children's Institute for Genomic Medicine, San Diego, CA, 92025, USA

15 68 Clinical Genetics Service, Nottingham University Hospitals NHS Trust, NG5 1PB,
16 Nottingham, UK

17 69 Human Genetics Centre of Excellence, Novo Nordisk Research Centre Oxford, Oxford, UK

18 70 Institute of Human Genetics, University Medical Center Göttingen, 37073, Göttingen,
19 Germany

20 71 Institute for Auditory Neuroscience and Inner EarLab, University Medical Center Göttingen,
21 37075, Göttingen, Germany

22 72 Neuroradiology Unit, IRCCS Istituto Giannina Gaslini, 16147, Genoa, Italy

23

24 Correspondence to: Reza Maroofian

25 Department of Neuromuscular Disorders, UCL Queen Square Institute of Neurology, London,
26 WC1N 3BG, UK

1 E-mail: r.maroo@ucl.ac.uk

2

3 Correspondence may also be address to: Gaurav K. Varshney

4 Genes & Human Disease Research Program, Oklahoma Medical Research Foundation,
5 Oklahoma City, OK, USA

6 E-mail: gaurav-varshney@omrf.org

7

8 **Running title:** *ACBD6*-related disease

9

10 **Keywords:** *ACBD6*; neurodegeneration; dystonia; ataxia; parkinsonism; *N*-myristoylation

11 **Abbreviations:** ACBDs=Acyl-CoA binding domain containing proteins; LCACoA=long-chain
12 fatty acyl-CoA esters; ACBD6=Acyl-CoA-binding domain-containing protein 6; ACBD5=Acyl-
13 CoA-binding domain-containing protein 5; ACB=Acyl-CoA binding; ANK=ankyrin repeat
14 domain; dpf=days post-fertilization; hpf=hours post-fertilization; NMT=*N*-myristoyltransferase;
15 Myr-CoA=myristoyl co-enzyme A; LOF=loss-of-function; PTZ=pentylentetrazole; VSR=visual
16 startle response; WES=whole exome sequencing; WISH=whole-mount in situ hybridization;
17 YnMyr=myristic acid alkyne; CRISPR =Clustered Regularly Interspaced Short Palindromic
18 Repeats GDD=global developmental delay; ID=intellectual disability

19

20 **Introduction**

21 Acyl-CoA-binding domain-containing proteins (ACBDs) are a large multigene family of
22 intracellular lipid-binding proteins, and in mammals, they include ACBD1-7. These proteins
23 specifically bind long-chain fatty acyl-CoA esters (LCACoA) and control their intracellular
24 concentration.^{1,2} Various cellular functions have been ascribed to this protein family, ranging
25 from lipid homeostasis, organelle formation, apoptotic responses, intracellular vesicle
26 trafficking, as well as tethering between the peroxisome and endoplasmic reticulum.² ACBDs
27 have been suggested to play a crucial role in brain development, via their strong proliferative

1 effects on the neural stem and progenitor cells.³ To date, defects in only two members of ACBDs
2 have been associated with Mendelian disorders in humans. *ACBD5* deficiency has been reported
3 to cause a combination of retinal dystrophy with leukodystrophy and defects in peroxisomal very
4 long-chain fatty acid metabolism in four families.⁴⁻⁷ *ACBD6* has been suggested as a candidate
5 gene for intellectual disability (ID) in two large-cohort gene discovery studies reporting limited
6 phenotypic data^{8,9} and in a case report describing 2 siblings with neurodevelopmental disorder,
7 obesity, pancytopenia, diabetes mellitus, cirrhosis, and renal failure but with a limited
8 neurological phenotype.¹⁰

9 The *ACBD6* protein has two domains: the N-terminal Acyl-CoA-binding (ACB) and the
10 specialized C-terminal ankyrin repeat (ANK) domain. This protein is detected in the cytosol and
11 nuclei of cells and modulates the acylation of lipids and proteins.¹¹ It has also been suggested
12 that *ACBD6* is associated with *N*-myristoyltransferase enzymes (NMTs) in human cells by
13 ligand binding and protein interaction, although direct evidence for this in cells is lacking.¹² In
14 humans, NMT1 and NMT2 enzymatically catalyze the *N*-myristoylation of substrate proteins by
15 transferring the myristate from myristoyl coenzyme A (Myr-CoA) onto the N-terminal glycine of
16 nascent proteins (co-translationally, at the ribosome) or to internal glycines uncovered by
17 protease cleavages during apoptosis (post-translationally).¹³ The global *N*-myristoylated
18 proteome consists of more than 200 co- and post-translationally *N*-myristoylated proteins in
19 humans,^{14,15} and *N*-myristoylation is important for the association of substrates with membranes
20 and their interaction with other proteins.¹⁶

21 Here, we describe 45 affected individuals from 28 unrelated families with 18 bi-allelic predicted
22 loss-of-function (LOF), 1 missense, and 1 in-frame insertion variants in *ACBD6* presenting a
23 new and distinct neurodevelopmental syndrome with a complex and progressive movement
24 disorder phenotype. We performed functional studies in zebrafish and *Xenopus tropicalis* (*X.*
25 *tropicalis*) knockouts generated by CRISPR/Cas9 that recapitulate many clinical features
26 reported in patients. We ruled out a major role for *ACBD6* in peroxisomes and investigated the
27 deregulation of co- and post-translationally *N*-myristoylated proteins in *ACBD6* deficient human,
28 zebrafish, and *X. tropicalis* cells, given its putative role in modulating NMT activity.

29

1 **Materials and methods**

2 **Patient identification and deep phenotyping**

3 By using the GeneMatcher platform,¹⁷ extensive international data sharing, and screening the
4 variant databases of several research and diagnostic laboratories worldwide, we identified 27
5 families with bi-allelic variants in *ACBD6*. Follow-up details were obtained in the family
6 reported by Yeetong *et al.* (2023).¹⁰ For a comprehensive phenotypic characterization of the
7 affected individuals, we obtained clinical details, including neurological examination, via a
8 universally-adopted proforma (Supplementary Table 1). Where possible, video recordings and
9 facial photographs of the affected individuals along with their brain MRIs were made available
10 for review by a movement disorders specialist (K.B.), dysmorphologist (M.S.), and
11 neuroradiologist (M.Sev.), respectively. Parents and legal guardians of all affected individuals
12 consented to the publication of clinical and genetic information, including video and
13 photographs, according to the Declaration of Helsinki, and the study was approved by the
14 respective local Ethics Committees.

16 **Genetic analysis**

17 Using genomic DNA from whole blood samples of the probands from the 28 unrelated families,
18 whole-exome sequencing (WES) was performed at 10 different centres worldwide with methods
19 specified in Supplementary Table 1. WES data analysis and variant filtering and prioritization
20 were performed using in-house implemented pipelines at different centres (Supplementary Table
21 1 for methods). Genotyping and homozygosity mapping were done in families 1, 3, 5, 7, and 21
22 according to standard procedures using the Automap software (<https://automap.iob.ch/>). Sanger
23 sequencing was performed to confirm co-segregation in all available family members. mRNA
24 expression analysis for *ACBD6* was performed by relative real-time PCR (Supplementary
25 Method 1). RNA studies to assay the effect of the splice acceptor site variants were performed as
26 previously described^{18,19} (Supplementary Methods 2).

27

28

1 **Functional studies in Zebrafish**

2 Zebrafish (*Danio rerio*) were raised and maintained under standard conditions in an AALAC
3 accredited facility at the Oklahoma Medical Research Foundation (OMRF). All experiments
4 were performed as per protocol 22-18 approved by the Institutional Animal Care Committee of
5 OMRF (IACUC). Wild-type zebrafish strain (*NHGRI-1*)²⁰ or transgenic lines as described were
6 used for all experiments. Detailed experimental procedures are described in Supplementary
7 Method 3.

8

9 **Functional studies in *Xenopus tropicalis***

10 *X. tropicalis* was used to test the gene-disease link for *ACBD6* further in a second animal model.
11 The details of *X. tropicalis* care, generating F0 *acbd6* crispant animals, and phenotypic analysis
12 of F0 *acbd6* crispant animals are provided in Supplementary Methods 4. All procedures were
13 conducted in accordance with the Home Office Code of Practice, under PP4353452 with
14 approval from the University of Portsmouth's Animal Welfare and Ethical Review Body.

15

16 **Cell culture**

17 Human fibroblasts were obtained from skin biopsies of two unrelated affected individuals, F1:S1
18 and F2:S1 with a single base change in *ACBD6* affecting the splice acceptor site in intron 5 and a
19 frameshift variant c.82dupG; p.(Val28GlyfsTer6), respectively. A control cell line from the
20 unaffected sibling from F1 (a homozygous wild-type sibling) was established (control 1). Wild-
21 type human control (C109) skin fibroblasts were provided by H. Waterham (control 2). COS-7
22 cells were cultured to perform immunofluorescence and microscopy analysis of *ACBD6*
23 localization (Supplementary Methods 5).

24

25

1 **Analysis of peroxisomal VLCFA β -oxidation parameters**

2 A D3-C22:0 loading test was performed by loading cells for 3 days with 30 μ M deuterated (D3)
3 C22:0 followed by fatty acid analysis with tandem mass spectrometry, essentially as previously
4 described.²¹

6 **YnMyr chemical proteomics, whole proteome analysis, and meta-** 7 **analyses**

8 Wild-type and ACBD6 deficient human fibroblasts, zebrafish, and *X. tropicalis* embryos were
9 metabolically labelled in the presence or absence of YnMyr, followed by unbiased whole
10 proteome analysis or chemical proteomics after YnMyr-enrichment to identify and quantify
11 proteins *N*-myristoylated with YnMyr. Sample preparation, processing, and data analyses were
12 performed as described previously, including the calculation of FDR adjusted P-values.^{22,23}
13 Meta-analysis for pathway- and disease-enrichment analysis were performed in Metacore
14 (Clarivate). Detailed experimental procedures are described in Supplementary Methods 6.

16 ***Acbd6* expression studies in mouse brain**

17 Gene expression in the adult mouse brain was performed and visualized as described in
18 Supplementary Method 7.

20 **Results**

21 Using WES and homozygosity mapping, we identified 20 homozygous variants in *ACBD6*
22 across 28 unrelated families. Variants were subjected to familial segregation testing (Fig. 1A)
23 and assessed using *in silico* analysis tools and genomic databases (Table 1 and Supplementary
24 Tables 1 and 2). All variants are listed using the canonical transcript NM_032360.4 (Fig. 1B).
25 Family 1 showed a splice variant (c.574-2A>G) which has been shown to result in cryptic splice
26 activation after 5 nucleotides in exon 6 (r.574_578del, p.(Arg193SerfsTer7) (Fig. 1C,

1 Supplementary Fig. 1)). Families 12 (c.694+1G>A) and 13 (c.664-2A>G) each harboured novel
 2 splice variants that resulted in skipping of exon 7, leading to a frameshift and premature
 3 termination (r.664_694del, p.(Asp222ProfsTer10). The (c.694+1G>A) variant showed additional
 4 evidence of activation of a cryptic splice donor site, also causing a frameshift and premature
 5 termination (r.694_694+1ins23, p.(Ala232AspfsTer8) (Fig. 1C, Supplementary Figure 2).
 6 Families 7 and 27, 8, 14, and 28 carried homozygous frameshift variants including c.474delA,
 7 p.(Asp159ThrfsTer16) (Families 7 and 27 shared this *ACBD6* variant); c.285delA,
 8 p.(Lys95AsnfsTer23); c.719_723delTTGTA, p.(Ile240ArgfsTer9); and c.360dupA,
 9 p.(Leu121ThrfsTer27), respectively. Families 2 and 21 shared the same homozygous frameshift
 10 *ACBD6* c.82dupG, p.(Val28GlyfsTer6) variant, as is the case with families 3, 16, and 17, who
 11 harboured the same homozygous frameshift *ACBD6* c.484_488delATATT, p.(Ile162Ter) variant.
 12 Families 4, 9, 11, 18, 20, 22, and 26 carried homozygous nonsense variants including c.760C>T,
 13 p.(Arg254Ter); c.594G>A, p.(Trp198Ter); c.539C>A, p.(Ser180Ter); c.217A>T, p.(Lys73Ter);
 14 c.160C>T, p.(Gln54Ter); c.280 C>T, p.(Gln94Ter); and c.216C>A, p.(Tyr72Ter), respectively.
 15 Families 5 and 15 shared the same homozygous nonsense *ACBD6* c.187G>T, p.(Glu63Ter)
 16 variant. Likewise, families 20 and 25 shared the same homozygous nonsense *ACBD6* c.160C>T,
 17 p.(Gln54Ter) variant. Families 23 and 24 each harboured a large deletion variant (c.664-
 18 18556_694+8366del, p.(?)) which spans 26,953bp of the *ACBD6* sequence and includes the
 19 complete deletion of exon 7. The affected individuals in family 6 carried an in-frame duplication
 20 variant c.654_656dupTAA, p.(Asn219dup) in exon 6. Families 10 and 19 harboured the same
 21 homozygous predicted-deleterious missense *ACBD6* variant c.602A>G, p.(Asp201Gly) in exon
 22 6 (Fig. 1D). All variants were ultra-rare or absent in ~1.8 million alleles inspected through a
 23 number of large genetic variant databases listed in Supplementary Table 2. A detailed description
 24 of the variants is provided in Supplementary Tables 1 and 2.

25

26 **Clinical delineation of *ACBD6*-related disease**

27 The cohort includes 23 male and 22 female affected individuals whose current ages widely range
 28 between 1 and 50 years. While almost half of the individuals (21/45) were <10 years old (the 1st
 29 age group), 11/45 (25%) individuals were between the ages of 10-19 years (the 2nd age group),
 30 and 13/45 (29%) affected individuals were ≥20 years old (the 3rd age group) at the most recent

1 review. Two siblings from Family 28 died at the ages of 31 and 30 due to stage 5 chronic renal
2 disease and aspiration, respectively. Almost all affected individuals are from consanguineous
3 unions with diverse ethnic backgrounds populating South and Central Asia, the greater Middle
4 East, Europe, and North and South America. Table 1 and Fig. 2A-D provide a summary of the
5 core phenotypic features of 45 affected individuals from 28 unrelated families with bi-allelic
6 *ACBD6* variants. A detailed phenotypic description is provided in Supplementary Table 1 and
7 Supplementary case reports. Video recordings are available from 16 families (Supplementary
8 videos 1-16).

9 Prenatal history was mostly unremarkable in the cohort and most of the affected individuals
10 reached normal gestational age. Head circumference at birth was \leq 3rd percentile in 7/21 (33%)
11 affected individuals. Head circumference on the latest available review was \leq the 2nd percentile
12 in 12/31 (39%) individuals and height was mostly below the age-adjusted average in the cohort
13 (18/32, 56%). Current weight was $>$ the 50th percentile in 20/34 (59%) affected individuals. All
14 patients manifested a moderate-to-severe global developmental delay (GDD) involving all
15 domains but predominantly affecting cognitive function and the acquisition of independent
16 walking and expressive language. While 10 patients had failed to acquire independent
17 ambulation by a mean age of 9.4 ± 5.0 years (age range 4-20), the mean age of independent
18 walking for the rest of the cohort was 3.7 ± 1.7 years (age range 1.5-8).

19 Upon the latest available follow-up, moderate-to-severe GDD/ID (45/45, 100%) with significant
20 expressive language impairment (40/41, 98% from non-verbal to a few words), movement
21 disorders (33/34, 97%), facial dysmorphism (38/40, 95%), and mild cerebellar ataxia (35/41,
22 85%) associated with limb spasticity/hypertonia (31/41, 76%) and gait abnormalities (33/35,
23 94%) were among the cardinal clinical features observed in the *ACBD6* cohort (Fig. 2C).

24 The most conspicuous and common movement disorder present in all the 3 age groups was
25 dystonia (30/32, 94%). This was frequently truncal dystonia leading to abnormal thoracic and/or
26 thoracolumbar spinal flexion (camptocormia) (30/31, 97%) and mild-to-moderate lateral flexion
27 of the trunk (Pisa syndrome, 22/32, 69%). Although the stooping of the body and its lateral
28 flexion were equally common in the 2nd (9/9 and 8/9, respectively) and the 3rd (10/10 and 10/10,
29 respectively) age groups, and were frequent in the 1st age group (10/12 and 4/12, respectively),
30 the severity of truncal dystonia suggested an age-dependent progression (Fig. 2B). Additionally,

1 some affected individuals developed mild upper limb action-induced dystonia (6/15, 40%), lower
2 limb dystonia (12/22, 55%), and cervical dystonia (8/26, 31%).

3 Another common hyperkinetic movement disorder in the cohort was a tremor. The upper limb
4 jerky tremor at rest and/or intention tremor was present in 22/35 (63%) affected individuals and
5 16/27 (59%) individuals had a mild head tremor. Dystonic head tremor, jerky tremor involving
6 all limbs, and negative myoclonus were also seen in a small number of patients. With advancing
7 age, parkinsonism/hypokinesia developed in 10/31 (32%) individuals, 6 of whom were over the
8 age of 20 years, and 4 cases were between ages 10-20 years. A trial of levodopa was done in
9 only 2 affected individuals with a minimal response. No other antiparkinsonian or anti dystonic
10 medication has been tried in the cohort. Additionally, subtle perioral muscle twitching and
11 stereotypic mouth dyskinesia were observed in the available video recordings of younger
12 affected individuals. Remarkably, simple motor and vocal tics and tic-like vocalizations were
13 detected in the video recordings of 7 young and adult cases (Supplementary Videos). Regarding
14 eye movements, limited upgaze (12/26, 46%), impaired saccades (9/19, 47%), and strabismus
15 (8/20, 40%) were frequent oculomotor abnormalities.

16 Lower limb spasticity, ascertained in 27/35 (77%) affected individuals, in combination with
17 cerebellar ataxia led to gait abnormalities described as a spastic-ataxic gait in 14 patients, and
18 clumsy/slow/broad-based or unstable gait in 17 individuals. Upper limb ataxia and spasticity
19 were confirmed in 13 and 9 affected individuals, respectively. Tendon release surgery was done
20 in 3 cohort members due to lower limb spasticity. Lower limb hypotonia was detected in single
21 isolated cases.

22 A deterioration in motor and cognitive abilities was reported in 28/28 (100%) affected
23 individuals suggesting a progressive disease course and underlying neurodegeneration. The
24 oldest member of the cohort, currently aged 50 years, has lost his ability to walk independently
25 and currently uses a wheelchair.

26 Complex partial, myoclonic, atonic, and generalized tonic-clonic seizures were reported in 13/39
27 (33%) patients with the seizure debut from neonatal age to 35 years old. Seizures were often
28 controlled with a combination of antiepileptic medications.

29 Younger affected individuals were reported to have hand stereotypies, and hyperactivity was
30 present in 9/21 (43%) patients. Signs of premature aging were seen in 9/38 (24%) individuals

1 from five families. Forty-six percent of patients had autistic features (13/28), temper tantrums
2 16/36 (44%), and aggressive behaviour (13/37, 35%) with a tendency to self-injury (6/34, 18%)
3 were reported. Sleep disturbances (15/33, 45%) were common, and urinary incontinence was
4 present in 15/24 (63%) individuals aged between 3-20 years.

5 Facial photographs were available from 32 affected individuals from 19 families (Fig. 2A). The
6 analysis of 19 children revealed the most frequent dysmorphic features including full nasal tip
7 (16/19), broad chin (14/19), bi-frontal/bi-temporal narrowing (12/19), hypertelorism (11/19), up-
8 slanting palpebral fissures (9/19), and depressed nasal bridge (9/19). Assessment of 13 adult
9 photos showed frequent signs such as a broad chin (11/13), full nasal tip (8/13), small mouth
10 (7/13), high nasal ridge (5/13), thin upper lip (5/13) and full lower lip (5/13) (more details in
11 Supplementary Tables 3 and 4).

12 Brain MRI scans were available for neuroradiological review in 29/45 subjects. The corpus
13 callosum was abnormal in 20/29 subjects (70%): partial or complete callosal agenesis was
14 observed in 7 individuals, while callosal hypoplasia with prevalent involvement of the posterior
15 sections was noted in the remaining 13 individuals. In 19/29 patients (66%), there was marked
16 hypoplasia/agenesis of the anterior commissure. Short midbrain and small inferior cerebellar
17 vermis were each detected in 11/29 affected individuals (38%). Mild to moderate reduction of
18 periventricular white matter with consequent ventriculomegaly was observed in 10/29 patients
19 (34%). In 7/29 (24%) individuals, incomplete hippocampal inversion was found. Finally, mild
20 hypertrophy of the Clava was noted in 5/21 (24%) individuals (Fig. 2D). Only 4/29 patients
21 (14%) had normal neuroimaging findings.

22

23 ***Acbd6* expression studies in mouse brain**

24 *Acbd6* is expressed in nearly all regions of the adult mouse brain profiled by single-cell RNA
25 sequencing (Supplementary Fig. 3).

26

27

1 **Characterization of ACBD6 LOF using CRISPR/Cas9-mediated** 2 **zebrafish mutant and F₀ knockout models**

3 Zebrafish *Acbd6* protein is highly conserved across species and displayed similar tissue-specific
4 expressions with humans (Supplementary Fig. 4). To examine the spatiotemporal expression
5 pattern, we performed whole-mount *in situ* hybridization (WISH) analysis and results revealed
6 that the *acbd6* mRNA was broadly expressed at 24 hours post-fertilization (hpf) and had elevated
7 expression levels in the central nervous system, developing eyes, otic vesicle, and trunk muscles
8 (Fig. 3A). Using CRISPR/Cas9 technology, we generated a genetic mutant of *acbd6*, and
9 through RT-qPCR analysis, verified a significant notable decrease in *acbd6* mRNA expression in
10 homozygous mutants (Supplementary Fig. 5A). During early embryonic developmental stages,
11 we did not observe any visible morphological abnormalities in homozygous mutants. However,
12 at the 6 days post-fertilization (dpf) stage, homozygous mutants (-/-) demonstrated a minor
13 reduction in eye size (~3%, indicated by the red line in Fig. 3B) compared to wild-type (+/+) or
14 heterozygous (+/-) animals (Fig. 3C). There was no significant change in head size (indicated by
15 the blue line in Fig. 3B) (Fig. 3D). The visual startle response (VSR) analysis²⁵ indicated that
16 reduced eye size impacts the visual function in *acbd6* -/- mutants (Fig. 3E). Furthermore, we
17 performed locomotion behaviour tests on mutants at 6 and 12 dpf in 10-minute intervals of light-
18 dark cycles (Fig. 3F-K and Supplementary Fig. 5-7, and detailed descriptions in Supplementary
19 Result 3). In general, *acbd6*-/- mutants exhibited a gradual decline in locomotor activity in dark
20 periods (Fig. 3F, G, I, J and Supplementary Fig. 7A, B, D, E) and an exaggerated response as
21 soon as lights are turned off at 6 dpf (Figs. 3F, H, Supplementary Fig. 5C-D and Supplementary
22 Fig. 7A, C), suggesting a hypertonia-like or spasticity behaviour.²⁶ As the larvae developed
23 further at 12 dpf, the *acbd6*-/- mutants showed an increase in distance moved after light on and
24 multiple locomotor bursts (Fig. 3I, K, Supplementary Fig. 6C and Supplementary Fig. 7D, F),
25 indicating light-induced seizure-like behaviour.²⁷ The mutants also demonstrated increased
26 mortality and severe developmental delay, with an overall reduction in brain size and disrupted
27 muscular phenotype (Fig. 3L, M). Histological analysis showed a reduction in brain size (Fig.
28 3N-W), particularly in regions such as the telencephalon, optic tectum, cerebellum, and retina
29 (Fig. 3O-Q, Fig. 3R-T, Fig. 3U-W, Supplementary Fig. 8A-C). Furthermore, skeletal muscle
30 fibres in *acbd6*-/- mutants displayed a disrupted phenotype, characterized by shortened and

1 scattered fibres and gaps (Supplementary Fig. 8D-F). Interestingly, adult *acbd6* $-/-$ mutant
2 survivors (Supplementary Fig. 9 and Supplementary video 17, 18) exhibited behavior resembling
3 that of individuals with an autism spectrum disorder.²⁸

4 To verify the specificity of the *acbd6* mutant phenotype, we utilized the F₀ knockout (also known
5 as F₀ crispant, or simply F₀) method to induce bi-allelic mutations and observed similar
6 morphological and molecular phenotypes in homozygous mutants and F₀ (Fig. 4A-D). We
7 discovered that F₀ also exhibited several phenotypes previously reported in affected individuals,
8 such as hypertelorism (Fig. 4E) and facial dysmorphism (broader chin; and wider lower jaw,
9 Supplementary Fig. 10A-H). These phenotypes were restored upon co-injection of wild-type
10 human mRNA, confirming the specificity of the phenotype. We also introduced the LOF
11 p.(Glu63Ter) and missense variants p.(Asp201Gly) into *acbd6* cDNA and observed impaired
12 protein function and failure to rescue the eye size phenotype (Fig. 4F) in F₀ knockouts. We
13 further investigated *acbd6* F₀ behaviour in light-dark cycles at 6- and 12-dpf and observed that
14 *acbd6* F₀ exhibited lower locomotor activity during dark periods (Fig. 4G, H) and an exaggerated
15 response after lights off, like homozygous mutants (Fig. 4G, I, and Supplementary Fig. 11A, B).
16 Additionally, *acbd6* F₀ exhibited light-induced seizure-like behaviour (red arrows in Fig. 4G and
17 Supplementary Fig. 11C, D). By 12 dpf, *acbd6* F₀ demonstrated reduced locomotor activity in
18 both light and dark periods (Supplementary Fig. 12A, B). These results suggest that *acbd6* F₀
19 larvae exhibit more severe abnormal locomotor behaviours than homozygous mutants. We
20 hypothesized that the loss of *acbd6* might increase susceptibility to chemical-induced seizures, as
21 observed in *acbd6* $-/-$ mutants showing seizure-like behaviour.^{29,30} To test this hypothesis, we
22 exposed *acbd6* F₀ and control larvae to different doses of the anticonvulsant drug,
23 pentylenetetrazole (PTZ), and discovered that *acbd6* F₀ larvae exhibited hyperexcited behaviour
24 at higher doses (Fig. 4J). This suggests that downregulation of *acbd6* may contribute to the onset
25 of epilepsy-like seizures. We examined the impact of *acbd6* F₀ on neuronal and skeletal muscle
26 development and discovered excessive axonal arborizations (Fig. 4K-N and Supplementary Fig.
27 13) and progressive degeneration of muscle fibres in *acbd6* F₀ larvae (Fig. 4O-T and
28 Supplementary Fig. 14). We also observed an increase in myelin basic protein a (*mbpa*)
29 expression in both *acbd6* F₀ and homozygous mutant (Supplementary Fig. 15A, B), which may
30 explain the abnormal axonal development phenotype. A detailed description of our results can be
31 found in the Supplementary Results 2. In summary, our zebrafish model replicated many of the

1 clinical features seen in individuals with bi-allelic variants in *ACBD6*, highlighting how these
2 variants may contribute to the progressive disease course. Our extensive analysis of both mutant
3 and F₀ in *acbd6* provides insight into the underlying mechanisms of the disease observed in
4 affected individuals.

6 ***Xenopus* ACBD6 F₀ knockout models**

7 *X. tropicalis* and humans have the same *acbd6* gene structures (Fig. 5A) and share 66% amino
8 acid identity (Supplementary Fig. 16A). Crispant F₀ tadpoles were produced by injection of two
9 non-overlapping sgRNAs targeting exon 1 of *acbd6* (Supplementary Fig. 16B). The effects were
10 specific, since both sgRNAs produced the same phenotype and when embryos with a SNP in the
11 PAM for one sgRNA were used, the embryos developed normally (Supplementary Fig. 17A, 3rd
12 upper panel from the left). ICE analysis³¹ of target amplicon sequences (Supplementary Fig.
13 16C) showed that at the gastrula stage, 74% of alleles in the embryos had indels, and that 63.5%
14 had a frameshift from a predominant 8bp deletion (sgRNA 68). For sgRNA71 the average was a
15 53.6% KO from a mix of indels. The range of phenotypes at later stages was due to distinct
16 levels of frameshift mutations among the groups (Supplementary Fig. 16D).

17 The first notable phenotype was gastrulation failure due to reduced cell movements (Fig. 5B and
18 Supplementary Fig. 17A). This limits the analysis of phenotypes at later stages since the
19 surviving embryos have been selected to have significantly greater mosaicism than normally
20 produced in this type of experiment. At swimming tadpole stages more than half of the crispants
21 had obvious craniofacial abnormalities (n = 36; Fig. 5C, Supplementary Fig. 17D, and Fig.17E)
22 and head measurement showed a decrease in the average area from 2.07 +/- 0.36 mm² in controls
23 to 1.52 +/- 0.27 mm² in crispants (t(34)=5.183, p<0.001; Fig. 5D). This was not a result of a
24 defect in the structure of the head cartilage, although when *in situ* it did appear constrained by
25 the overall head structure (compare Fig. 5E (control) and F (crispant)). The cartilage components
26 were nonetheless present and morphologically normal upon dissection; however, the overall
27 cartilage size was smaller than controls consistent with the observed microcephaly. To detect
28 subtler changes in head structure, we compared control and crispant tadpoles by MicroCT (Fig.
29 5G). Three things were apparent in the three embryos selected at random from the crispant
30 group: first, the eyes (yellow arrows) were abnormal and displaced (e.g. the dorsal and frontal

1 views in the right-hand panel) and in one case there was anophthalmia, the latter was rare
2 because it was not detected in the bright field images. Second, a muscle in the face was poorly
3 developed or absent (red arrows). From comparison with *X. laevis* staining,³² we tentatively
4 identified this as the geniohyoidius, although the muscle seems more distant from the midline in
5 *X. tropicalis* than in *X. laevis*. The brain also has obvious structural abnormalities which are most
6 pronounced in the midbrain (blue arrows). Comparing the movement of control and *acbd6*
7 crispant tadpoles showed that the crispants move less over a 10-minute period (average 2.37
8 mm/s for controls and 1.01 mm/s for crispants, n = 50). The difference was statistically
9 significant (t(78)=4.9, p<0.001) (Fig. 5H) (Supplementary videos 19-22). After the deaths at
10 gastrulation, crispants and control embryos survived similarly until the feeding stage (Fig. 5I).

11

12 **Loss of ACBD6 does not impact peroxisome function**

13 Several members of the ACBD family have been linked to peroxisome function.² Furthermore,
14 peroxisomal dysfunction is linked to developmental defects and neurological abnormalities.³³ To
15 investigate if peroxisomal parameters were altered in *ACBD6* deficiency, patient (from F1:S1
16 and F2:S1) and control (F1:II-2 unaffected sibling; wild type C109) fibroblasts were processed
17 for immunofluorescence using antibodies against the peroxisomal membrane marker PEX14 and
18 catalase, a peroxisomal matrix protein (Fig. 6 A, B). No alterations in peroxisome protein import,
19 morphology, distribution, or number were observed when compared to control fibroblasts (Fig. 6
20 A, B). In addition, expression of a Myc-ACBD6 construct in COS-7 cells confirmed a
21 cytoplasmic and nuclear localisation of Myc-ACBD6,³⁴ but did not provide evidence for a
22 peroxisomal localisation under standard culture conditions (Fig. 6C). In addition, fatty acid
23 analysis after a D3-C22:0 loading test in cultured fibroblasts did not reveal any abnormalities of
24 peroxisomal VLCFA β -oxidation (Supplementary Table 5) as observed in *ACBD5* deficiency.^{5,33}
25 Detailed results are described in Supplementary Results 3.

26

27

1 **Investigation of the effect of *ACBD6* deficiency on *N*-myristoylation** 2 **in patient-derived fibroblasts**

3 We employed a chemical proteomic approach to identify and quantify *N*-myristoylated proteins,
4 by combining metabolic labelling of living cells with YnMyr,¹⁴ an alkyne-containing myristic
5 acid analogue, and Click chemistry-enabled enrichment of YnMyr-labelled proteins, coupled to
6 mass spectrometry proteomics analysis.²² Chemical proteomics revealed 68 known co-
7 translationally, and 18 post-translationally *N*-myristoylated proteins expressed in the fibroblasts
8 derived from F1:S3 and his healthy sibling (Supplementary Fig. 18A, B, respectively). As
9 expected, the incorporation of YnMyr was markedly reduced by treatment with 100 nM IMP-
10 1088, a selective and highly potent NMT inhibitor,^{23,35} in both the fibroblasts of the healthy
11 control and the patient, confirming the specificity of labelling (Supplementary Fig. 18C, D,
12 respectively). Proteins co- and post-translationally *N*-myristoylated with YnMyr were detected in
13 significantly higher abundance in the patient-derived fibroblasts compared to the healthy sibling
14 (Supplementary Fig. 18E), suggesting *ACBD6* deficiency provokes increased incorporation of
15 YnMyr, potentially through increased *N*-myristoylation or upregulation of lipid salvage
16 pathways leading to increased YnMyr import (Fig. 6D). We hypothesise this may be caused by
17 the differential interplay of the two *N*-myristoyltransferases (NMT1 and NMT2) with *ACBD6*
18 for various substrates. Although fibroblasts from only one affected individual and a healthy
19 sibling were compared, the apparent differential *N*-myristoylation warrants more detailed
20 investigations of the role of *ACBD6* in *N*-myristoylation in cell types involved in the described
21 human clinical phenotypes.

23 **Proteomics analyses of developing wild-type and *acbd6* crispant** 24 **zebrafish**

25 To shed light on the potential role of *acbd6* on *N*-myristoylation during zebrafish development,
26 we employed metabolic labelling with YnMyr and chemical proteomics at different stages of
27 development. At 72 and 120 hpf, both wild-type and *acbd6* crispant zebrafish express >32
28 significantly enriched proteins, for each of which the human orthologue is a validated co-
29 translationally *N*-myristoylated substrate (Supplementary Figs. 19A-D). In addition, significantly

1 enriched proteins also included >48 proteins with N-terminal glycine, thereby potentially *N*-
2 myristoylated, but where unequivocal evidence of *N*-myristoylation is currently lacking the
3 human orthologue, or where the human orthologue does not possess an N-terminal glycine. At 72
4 hpf, an increased abundance of YnMyr-labelled proteins is observed in the *acbd6* crispant,
5 including Marcks and Chchd-related proteins, known to be co-translationally *N*-myristoylated in
6 humans (Fig. 7A). Of note, zebrafish express duplications of multiple proteins, including the
7 aforementioned Marcks and Chchd-related proteins (Fig. 7A). Conversely, enrichment of several
8 zebrafish proteins with N-terminal glycine in zebrafish but not found with a N-terminal glycine
9 in humans was significantly reduced in *acbd6* crispants, including Sfpq, associated with brain
10 development, CNS neuron axonogenesis and midbrain-hindbrain boundary initiation (Fig. 7A).
11 Similar increases in Marcks and Chchd-related proteins are observed in the *acbd6* crispants at
12 120 hpf, whereas Fus and Fusl are further decreased (Fig. 7B).

13 We next performed a whole proteomics analysis comparing wild-type and *acbd6* crispant at 72
14 and 120 hpf (Supplementary Figs. 19E, F, respectively). In contrast to the significant increase of
15 YnMyr labelling observed in *acbd6* crispants (Figure 7A, B), the abundance of *N*-myristoylated
16 proteins such as Marcks and Chchd-related proteins is not significantly increased at the whole
17 proteome level at 72 and 120 hpf, further indicating the role of *acbd6* on the process of *N*-
18 myristoylation in zebrafish. Meta-analysis of up-regulated proteins in *acbd6* crispants revealed a
19 significant involvement of translation- and metabolism-related pathways (Supplementary Fig.
20 20A), and significant enrichments in disease networks including frontotemporal dementia and
21 delayed speech and language development (Supplementary Fig. 20B). Down-regulated proteins
22 are significantly involved in pathways related to nervous system development, as well as
23 neurodegeneration (Fig. 7C). Enriched disease-related networks include dystonia muscle
24 spasticity and movement disorders, a striking similarity with the observations in affected
25 individuals (Supplementary Fig. 20C). At 120 hpf, a meta-analysis of the whole proteome data
26 reveals similar enrichments (Supplementary Fig. 20D-G). Notably, upregulated proteins enrich
27 in translation- and metabolism-related pathways, whereas downregulated proteins further enrich
28 in pathways of neurological development and disease, including spasticity (Supplementary Fig.
29 20G).

30

1 **Proteomics analyses of developing wild-type and *acbd6* crispant *X.*** 2 ***tropicalis***

3 Similar to the chemical proteomics analyses in zebrafish, we used YnMyr labelling to identify *N*-
4 myristoylated substrates and the pathways affected by the loss of *acbd6* in developing *Xenopus*.
5 Here, wild-type, crispant 68 or crispant 71 *X. tropicalis* were metabolically labelled from 1 hpf to
6 18 hpf, due to the previously reported growth arrest. Chemical proteomics of YnMyr labelling
7 revealed >10 *X. tropicalis* proteins the human orthologues of which are known to be co-
8 translationally *N*-myristoylated, including a duplication of Marcks, as well as *X. tropicalis*
9 proteins which share the N-terminal glycine with their orthologue in humans (Supplementary
10 Fig. 21A-C). Comparing wild-type with *acbd6* crispant 68 and 71 (Figs. 7D and E, respectively)
11 reveals a marked depletion of YnMyr-labelled proteins in the crispants, including all identified
12 *X. tropicalis* proteins with co-translationally *N*-myristoylated human orthologues. Both crispants
13 reveal prominent and significant reductions in proteins including Marcks, Ppm1b, Ppm1g. Whole
14 proteome analysis revealed Marcks and Fus are markedly reduced in *acbd6* crispant 68, while
15 Ppm1a is slightly increased, and in *acbd6* crispant 71, both Marcks and Ppm1b are reduced
16 (Supplementary Figs 21D, E). Meta-analysis (Supplementary Fig. 22) revealed upregulated
17 proteins in crispants 68 and 71 are significantly affected in pathways of translation and
18 metabolism, and notably, the 'Parkinson-disease'-specific disease network was significantly
19 enriched (Fig. 7F).

20 **Discussion**

21 **A neurodevelopmental syndrome with progressive movement** 22 **disorders characterizes *ACBD6*-related disease**

23 Despite their predicted roles in cellular lipid metabolism, the functions of many of the ACBDs
24 still remain unclear, as is the consequence of ACBD protein defects on human pathophysiology.
25 In this study, we identified novel and ultra-rare bi-allelic predicted LOF variants in *ACBD6* as
26 the disease cause in 45 previously undiagnosed individuals from 28 unrelated families. A wide
27 age range of the cohort members (1-50 years) delineated the age-related clinical spectrum and
28 the natural history of the *ACBD6*-related disease. The disease had an invariably early-onset and

1 inevitably progressive course with significant motor and cognitive deterioration upon reaching
2 adulthood, a course suggestive of underlying neurodegeneration. The phenotype is complex
3 involving the constellation of extrapyramidal, pyramidal, and cerebellar ataxia symptoms
4 associated with GDD/ID, microcephaly, and variable epilepsy. Impaired expressive language,
5 delayed gait acquisition, and early-onset stooped posture with lateral trunk flexion (Pisa
6 syndrome) were among the important pathognomonic features. Additionally, tics and tic-like
7 vocalizations seen in 6 affected individuals are peculiar features associated with several
8 neurological disorders, particularly with chorea-acanthocytosis.³⁶ Whilst the present cohort of
9 patients with *ACBD6*-related disease did have facial dysmorphism, it did not suggest a
10 recognizable facial "gestalt". The most common dysmorphic feature in the cohort was a broad
11 chin. Of note, most of the patients had hypoplasia/agenesis of the corpus callosum and anterior
12 commissure, suggesting a potential role for *ACBD6* in axonal pathfinding and corpus callosum
13 development. Interestingly, claval hypertrophy observed in the present cohort is a well-
14 documented neuroradiological sign of *PLA2G6*-associated neurodegeneration.³⁷

15 Defects in numerous genes and pathways are known to present with the constellation of
16 symptoms observed in *ACBD6*-related disease, particularly, with various combinations of
17 dystonia, parkinsonism, ataxia, and spasticity.³⁸⁻⁴¹ Their clinical phenotypes are typically
18 classified according to the predominating symptom; however, a later approach tends to define
19 this with a spectrum of genetic dystonia-ataxia, parkinsonism-dystonia/ataxia, and ataxia-
20 spasticity syndromes.³⁸⁻⁴¹ Thus, several forms of complicated hereditary spastic paraplegia,
21 spastic ataxia, and young-onset dystonia-parkinsonism syndromes may overlap with *ACBD6*
22 phenotypes. A suggested differential diagnosis with the disease pathways involved is given in
23 Supplementary Table 7.

24 It has been suggested that neurodevelopmental abnormalities and neurodegeneration could share
25 several molecular and cellular mechanisms. For instance, proteins, such as A β , MAPT/tau, Rac1,
26 Progranulin, Huntingtin, PINK, and Parkin, frequently implicated in Alzheimer's disease,
27 Parkinson's disease, and Huntington's diseases are important for nervous system development.⁴²
28 A wide range of multisystem genetic disorders could present with a biphasic course where
29 complex neurological phenotype gradually evolves on the background of a pre-existing
30 neurodevelopmental disorder.^{43,44} Therefore, we propose a likely clinical continuum associated

1 with *ACBD6*-related disease, characterized by a combination of neurodevelopmental
2 abnormalities and neurodegeneration.

3

4 **Zebrafish *acbd6* knockouts recapitulate many features observed in** 5 **affected individuals**

6 In recent years, the zebrafish has gained significance as an animal model for investigating
7 neurodevelopmental disorders, owing to its high physiological similarity to humans and its
8 responsiveness to genetic and pharmacological interventions.^{45,46} The acyl-CoA binding domain
9 of human and zebrafish ACBD6 share significant identity and similarity in the ankyrin-repeat
10 motif and acyl-CoA binding domain, with 80% identity and 95.4% similarity in the former and
11 69.2% identity and 78.2% similarity in the latter. Zebrafish models for ACBD proteins do not
12 currently exist; however, by generating *acbd6* knockouts in zebrafish, we observed similar
13 phenotypes to those of affected individuals, such as movement disorders, seizures, and facial
14 dysmorphism. Our findings suggest that *acbd6* is critical for animal development, as the loss of
15 this protein results in severe global developmental delay and increased mortality over time, as
16 evidenced by stunted growth and severe brain development impairment by 30 dpf. Moreover, we
17 observed motor neuron over-branching during development and progressive muscle loss,
18 suggesting a combination of muscle and neuronal degeneration leading to movement
19 abnormalities. Furthermore, the knockout zebrafish demonstrated increased locomotor behaviour
20 in the dark, potentially indicating seizure or anxiety-like behaviour, similar to that seen in
21 affected patients. In summary, the *Acbd6* zebrafish models offer a promising tool for gaining
22 deeper mechanistic insights into the role of *acbd6* and for screening potential therapeutic
23 interventions, as zebrafish are ideal for high-throughput *in vivo* drug screening. As such, the
24 *acbd6* model represents a valuable resource for drug discovery research.

25

26

1 ***X. tropicalis acbd6* knockouts have gastrulation failure, brain** 2 **defects, and reduced locomotion**

3 *X. tropicalis* is a diploid clawed frog with a genome that contains over 80% of identified human
4 disease genes and importantly is syntenic with over two-thirds of the human genome.⁴⁷ Features
5 of this animal include rapid external development and a transparent tadpole. A deep
6 understanding of *Xenopus* biology throughout the last 70 years,⁴⁸ combined with ease of genetic
7 manipulation⁴⁹, makes it powerful for modeling disease genes^{50,51} and understanding genetic
8 disease mechanisms.⁵²⁻⁵⁵

9 In the present study, the inactivation of *acbd6* in *X. tropicalis* caused severe cell movement
10 failures during gastrulation. Marcks requires *N*-myristoylation to act in early development⁵⁶ and
11 is required for normal cell movement during gastrulation in frog.⁵⁷ It is interesting to speculate
12 that the loss of *acbd6* may cause gastrulation defects due to a loss of Marcks *N*-myristoylation;
13 an aspect that requires future work. Due to embryo deaths at gastrula stages, a caveat for the
14 interpretation of the subsequent phenotype analysis is the unusually high mosaicism of these
15 crisant tadpoles. Despite this, there were clear phenotypic differences between the control and
16 crisant tadpoles. In some cases, the change predominated in one-half of the tadpole due to
17 mosaicism (on the L-R axis, see for example Fig. 5G second image from the left). These
18 differences included microcephaly, reduced movement, eye abnormalities, and brain structure
19 differences, data that strengthen the link between *ACBD6* variants and the pathology observed in
20 the patient cohort.

21 22 ***ACBD5* and *ACBD6* have different cellular localizations but both** 23 **genes exhibit a neurodegenerative phenotype**

24 *ACBD5* is a peroxisomal membrane protein. Although current knowledge of the phenotype
25 associated with *ACBD5* defects is limited to only four reported families,⁴⁻⁷ similar to *ACBD6*,
26 individuals with defective *ACBD5* seem to exhibit a neurodegenerative disease, albeit with a
27 different range of associated symptoms. Our study on peroxisome morphology and function with
28 *ACBD6* deficient and control fibroblasts did not reveal significant alterations as has been

1 demonstrated in ACBD5 deficiency. Furthermore, Myc-ACBD6 did not localize to peroxisomes
2 when expressed in COS-7 cells.

3

4 **ACBD6 deficiency alters myristate probe YnMyr incorporation into** 5 **substrates of NMT**

6 Our chemical proteomics analysis comparing *N*-myristoylated proteins in fibroblasts, derived
7 from a patient and their healthy sibling, revealed significant differences in YnMyr-labelled
8 proteins. YnMyr incorporation was significantly higher in the ACBD6-deficient patient
9 fibroblasts, spanning 68 known co- and 18 post-translationally *N*-myristoylated proteins.
10 Interestingly, an apparent differential variation of YnMyr incorporation in the identified NMT
11 substrates between healthy and patient fibroblasts was also observed. Our investigation in
12 ACBD6 deficient fibroblasts might indicate its role in *N*-myristoylation of a subset of NMT
13 substrates, but further studies are required to investigate this putative role of ACBD6.
14 Furthermore, to study the effect of ACBD6 deficiency on *N*-myristoylation, future analyses will
15 need to focus on cell types likely directly impacting the pathways involved in *e.g.* neurological
16 development.

17 Both the zebrafish and *X. tropicalis* model systems recapitulate many of the identified human
18 phenotypes, including movement disorders, seizures, facial dysmorphology, and developmental
19 defects. This evidence for notable evolutionary conservation of ACBD6 function across
20 mammals, amphibia, and teleosts emphasizes the power of multiple, non-mammalian models as
21 a method for rapid and cost-effective human gene analysis. Through our chemical proteomics
22 analysis, coupled with whole proteome and meta-analysis, we identified that *acbd6*-deficiency in
23 developing zebrafish embryos results in a prominent increase in metabolic labelling of known
24 co- and post-translationally *N*-myristoylated proteins with YnMyr, suggesting *N*-myristoylation
25 is dependent on a direct or indirect interaction between *acbd6* and the *N*-myristoyltransferases.
26 Meta-analysis furthermore revealed that *acbd6* deficiency provokes an overall increase of
27 proteins *N*-myristoylated with YnMyr, with a subset involved in the development of the eye,
28 neuron and muscle, being reduced. Overall, this suggests that ACBD6 is involved in the *N*-
29 myristoylation of a subset of *N*-myristoyltransferase substrates that require modification, and

1 might indicate activation of a rescue mechanism in response to loss of *ACBD6*. Concomitantly,
2 potentially compromised myristic acid-CoA binding and shuttling to *N*-myristoyltransferases in
3 *ACBD6*-deficient cells may upregulate salvage pathways to increase cellular myristate
4 concentration. For example, acyl-CoA synthases can activate exogenous lipids directly,
5 potentially bypassing or compensating loss of *ACBD6*. In this case, YnMyr-CoA could more
6 effectively compete with endogenous myristic acid-CoA for protein *N*-myristoylation than in
7 healthy subjects, leading to the observed enhanced YnMyr labelling, suggesting exogenous
8 myristic acid supplementation through dietary supplementation might have the potential to
9 reduce the burden of *ACBD6* deficiency. The determined differences in protein *N*-myristoylation
10 between the skin fibroblasts derived from a single patient and unaffected sibling align with the
11 YnMyr chemical proteomics findings from our zebrafish study. Consequently, the YnMyr
12 chemical proteomics data of the human patient and unaffected fibroblast serves only as
13 qualitative confirmatory evidence of the zebrafish study. For this purpose, we did not seek
14 further replication of these findings across multiple patient cell lines.

15 In contrast to *ACBD6* deficient human fibroblasts and zebrafish crispants, the *acbd6 X. tropicalis*
16 crispants show a prominent and significant reduction of YnMyr labelling, including proteins
17 such as Marcks, Chchd, Ppm1b, Ppm1g, and Fus, which are significantly involved in
18 development. Meta-analysis indicates the upregulation of neurological and sight-related disease
19 networks upon *acbd6* loss. The significant effect of *acbd6* loss on *X. tropicalis* development at
20 the gastrula stage precludes a clear interpretation of the effect of *acbd6* knockout on *N*-
21 myristoylation due to the presence of confounding changes in other processes during the period
22 of metabolic labelling. The clearly non-viable state of the *X. tropicalis* embryos likely leads to
23 defects in lipid metabolism, protein translation and related processes over this period which go
24 beyond the direct impact of *acbd6* on cells.

25 In summary, we have shown that bi-allelic pathogenic variants in *ACBD6* are associated with a
26 new and distinct neurodevelopmental disease with a complex and progressive dystonia-
27 parkinsonism-ataxia phenotype. Zebrafish and *X. tropicalis* crispants recapitulate the main
28 clinical features of the cohort with affected pathways underlying translation, metabolism,
29 neurological development, and neurological diseases. Further studies are warranted to delineate
30 the clinical phenotype and understand the pathomorphological presentation and molecular
31 mechanisms of the *ACBD6*-related disease. This includes elucidating the molecular interplay

1 between ACBD6 and *N*-myristoyltransferases involved in the co- and post-translational
2 modification of nascent protein chains, how ACBD6 affects lipid metabolism and the
3 identification of treatments of ACBD6 deficiency.

4

5 **Data availability**

6 The data that support the findings of this study are available from the corresponding author, upon
7 reasonable request. The mass spectrometry proteomics data have been deposited to the
8 ProteomeXchange Consortium via the PRIDE²⁴ partner repository with the dataset identifiers
9 PXD024957 (YnMyr chemical proteomics in human cells), PXD043676 (YnMyr chemical
10 proteomics in zebrafish), PXD043679 (zebrafish whole proteome), PXD043677 (YnMyr
11 chemical proteomics in *X. tropicalis*) and PXD043680 (*X. tropicalis* whole proteome).

12

13 **Acknowledgements**

14 The authors are grateful to the families for their support and consent to the publication of this
15 study. The families were recruited as part of the SYNAPS Study Group collaboration funded by
16 The Wellcome Trust and strategic award (Synaptopathies) funding (WT093205 MA and
17 WT104033AIA). This research was conducted as part of the Queen Square Genomics group at
18 University College London, supported by the National Institute for Health Research University
19 College London Hospitals Biomedical Research Centre. We thank Prof. Zimmer,
20 Neuroradiology Technical University of Munich for providing MRI scans. We would like to
21 thank A. Le Quang for generation of the Myc-ACBD6 construct and J. Passmore for support
22 with peroxisome quantification. R.G. and A.V. are members of the European Reference
23 Networks EpiCARE and ITHACA. S. R.-S. is a member of the European Reference Network
24 EURO NMD.

25

1 **Funding**

2 This study was funded by the MRC (MR/S01165X/1, MR/S005021/1, G0601943,
3 MR/V012177/1), The National Institute for Health Research University College London
4 Hospitals Biomedical Research Centre, Rosetree Trust, Ataxia UK, MSA Trust, Brain Research
5 UK, Sparks GOSH Charity, Muscular Dystrophy UK (MDUK), Muscular Dystrophy
6 Association (MDA USA). M.Schr. is supported by the BBSRC (BB/N01541X/1, BB/T002255/1,
7 BB/W015420/1) and the European Union's Horizon 2020 research and innovation programme
8 under the Marie Skłodowska-Curie grant agreement No 812968 PERICO (to M.Schr., H.W.).
9 R.K. is supported by the Rosetrees Trust PhD Plus award (PhD2022\100042). H.H. and R.K. are
10 supported by Global Parkinson's Genetic Program (GP2) MJFF Grant ID: MJFF-022153. B.V. is
11 supported by Intramural Funding (fortune) at the University of Tübingen (2545-1-0.), the
12 Ministry of Science, Research and Art Baden-Württemberg and the German Research
13 Foundation VO 2138/7-1 grant 469177153 as well as through the Collaborative Research Center
14 889 and the Multiscale Bioimaging Cluster of Excellence (MBExC). The European Commission
15 (Marie Skłodowska Curie Individual Fellowship grant 752165 to W.W.K.), EPSRC (Impact
16 Acceleration Account grant PS1042 to W.W.K. and E.W.T.), Cancer Research UK
17 (C29637/A21451 and C29637/A20183 to E.W.T.). Work in the E.W.T. laboratories is supported
18 by the Francis Crick Institute, which receives its core funding from Cancer Research UK
19 (FC001057 and FC001097), the UK Medical Research Council (FC001057 and FC001097), and
20 the Wellcome Trust (FC001057 and FC001097). M.Shm. acknowledges funding from the
21 Deutsche Forschungsgemeinschaft (DFG, German Research Foundation) – Project-ID
22 431984000 – SFB 1453 (CRC Nephgen) and Excellence Initiative CIBSS - EXC-2189 - Project
23 ID 390939984. R.G. is supported by the Tuscany Region Call for Health 2018 (grant DECODE-
24 EE) and the Brain project by Fondazione CA.RI.FI. G.K.V. is supported by a grant from
25 Oklahoma Medical Research Foundation, USA. These results reported here were generated using
26 funding received from the Solve-RD project within the European Rare Disease Models &
27 Mechanisms Network (RDMM-Europe). The Solve-RD project has received funding from the
28 European Union's Horizon 2020 research and innovation programme under grant agreement No
29 779257 (G.K.V., R.M., H.H.). Department of Public Genetics - Israeli MOH (A.S.). Work at the
30 EXRC is supported by the BBSRC (BB/R014841/1) and Wellcome Trust (212942/Z/18/Z).

1 Work in the laboratory of J.R.L. is funded in part by US National Institutes of Health (NINDS
2 NS105078; NHGRI HG011758) and the Spastic Paraplegia Foundation. R.W.T. is funded by the
3 Wellcome Centre for Mitochondrial Research (203105/Z/16/Z), the Mitochondrial Disease
4 Patient Cohort (UK) (G0800674), the Medical Research Council International Centre for
5 Genomic Medicine in Neuromuscular Disease (MR/S005021/1), the Medical Research Council
6 (MR/W019027/1), the Lily Foundation, the Pathological Society, the UK NIHR Biomedical
7 Research Centre for Ageing and Age-related disease award to the Newcastle upon Tyne
8 Foundation Hospitals NHS Trust and the UK NHS Highly Specialized Service for Rare
9 Mitochondrial Disorders of Adults and Children. V.Sh. is supported by Thailand's Health
10 Systems Research Institute (HSRI 66-122). Y.J. is supported by Newlife Charity grant (SG/18-
11 19/02). M.Ily. was funded through HEC-NRPU grant (17341). For the purpose of Open Access,
12 the author has applied a CC BY public copyright license to any Author Accepted Manuscript
13 version arising from this submission.

14

15 **Competing interests**

16 E.W.T. is a director and shareholder of Myricx Pharma Ltd, and an inventor on a patent
17 application describing NMT inhibitors including IMP-1088 (Bell, AS; Tate, EW; Leatherbarrow,
18 RJ; Hutton, JA; Brannigan, JA, "Compounds and their use as inhibitors of *N*-myristoyl
19 transferase", PCT In Appl (2017) WO 2017001812). E.A.N. is an employee of GeneDx, LLC.
20 J.R.L. holds stock in 23andMe and is a consultant for Genome International. Y.J. is an employee
21 of Novo Nordisk.

22

23 **Supplementary material**

24 Supplementary material is available at *Brain* online.

25

26

1 **References**

- 2 1. Neess D, Bek S, Engelsby H, Gallego SF, Faergeman NJ. Long-chain acyl-CoA esters in
3 metabolism and signaling: Role of acyl-CoA binding proteins. *Prog Lipid Res.* Jul 2015;59:1-25.
4 doi:10.1016/j.plipres.2015.04.001
- 5 2. Islinger M, Costello JL, Kors S, *et al.* The diversity of ACBD proteins - From lipid
6 binding to protein modulators and organelle tethers. *Biochim Biophys Acta Mol Cell Res.* May
7 2020;1867(5):118675. doi:10.1016/j.bbamcr.2020.118675
- 8 3. Bi J, Mischel PS. Acyl-CoA-Binding Protein Fuels Gliomagenesis. *Cell Metab.* Aug 6
9 2019;30(2):229-230. doi:10.1016/j.cmet.2019.07.007
- 10 4. Abu-Safieh L, Alrashed M, Anazi S, *et al.* Autozygome-guided exome sequencing in
11 retinal dystrophy patients reveals pathogenetic mutations and novel candidate disease genes.
12 *Genome Res.* Feb 2013;23(2):236-47. doi:10.1101/gr.144105.112
- 13 5. Bartlett M, Nasiri N, Pressman R, Bademci G, Forghani I. First reported adult patient
14 with retinal dystrophy and leukodystrophy caused by a novel ACBD5 variant: A case report and
15 review of literature. *Am J Med Genet A.* Apr 2021;185(4):1236-1241. doi:10.1002/ajmg.a.62073
- 16 6. Ferdinandusse S, Falkenberg KD, Koster J, *et al.* ACBD5 deficiency causes a defect in
17 peroxisomal very long-chain fatty acid metabolism. *J Med Genet.* May 2017;54(5):330-337.
18 doi:10.1136/jmedgenet-2016-104132
- 19 7. Gorukmez O, Havali C, Gorukmez O, Dorum S. Newly defined peroxisomal disease with
20 novel ACBD5 mutation. *J Pediatr Endocrinol Metab.* Jan 27 2022;35(1):11-18.
21 doi:10.1515/jpem-2020-0352
- 22 8. Najmabadi H, Hu H, Garshasbi M, *et al.* Deep sequencing reveals 50 novel genes for
23 recessive cognitive disorders. *Nature.* Sep 21 2011;478(7367):57-63. doi:10.1038/nature10423
- 24 9. Hu H, Kahrizi K, Musante L, *et al.* Genetics of intellectual disability in consanguineous
25 families. *Mol Psychiatry.* Jul 2019;24(7):1027-1039. doi:10.1038/s41380-017-0012-2
- 26 10. Yeetong P, Tanpowpong N, Rakwongkhachon S, Suphapeetiporn K, Shotelersuk V.
27 Neurodevelopmental Disorder, Obesity, Pancytopenia, Diabetes Mellitus, Cirrhosis, and Renal

- 1 Failure in ACBD6-Associated Syndrome A Case Report. *Neurol-Genet.* Feb
2 2023;9(1)doi:ARTN e200046
3 10.1212/NXG.000000000200046
- 4 11. Soupene E, Kuypers FA. Ligand binding to the ACBD6 protein regulates the acyl-CoA
5 transferase reactions in membranes. *J Lipid Res.* Oct 2015;56(10):1961-71.
6 doi:10.1194/jlr.M061937
- 7 12. Soupene E, Schatz UA, Rudnik-Schoneborn S, Kuypers FA. Requirement of the acyl-
8 CoA carrier ACBD6 in myristoylation of proteins: Activation by ligand binding and protein
9 interaction. *PLoS One.* 2020;15(2):e0229718. doi:10.1371/journal.pone.0229718
- 10 13. Losada de la Lastra A, Hassan S, Tate EW. Deconvoluting the biology and druggability
11 of protein lipidation using chemical proteomics. *Curr Opin Chem Biol.* Feb 2021;60:97-112.
12 doi:10.1016/j.cbpa.2020.10.002
- 13 14. Thinon E, Serwa RA, Broncel M, *et al.* Global profiling of co- and post-translationally N-
14 myristoylated proteomes in human cells. *Nat Commun.* Sep 26 2014;5:4919.
15 doi:10.1038/ncomms5919
- 16 15. Castrec B, Dian C, Ciccone S, *et al.* Structural and genomic decoding of human and plant
17 myristoylomes reveals a definitive recognition pattern. *Nat Chem Biol.* Jul 2018;14(7):671-679.
18 doi:10.1038/s41589-018-0077-5
- 19 16. Meinnel T, Dian C, Giglione C. Myristoylation, an Ancient Protein Modification
20 Mirroring Eukaryogenesis and Evolution. *Trends in Biochemical Sciences.* Jul 2020;45(7):619-
21 632. doi:10.1016/j.tibs.2020.03.007
- 22 17. Sobreira N, Schiettecatte F, Valle D, Hamosh A. GeneMatcher: a matching tool for
23 connecting investigators with an interest in the same gene. *Hum Mutat.* Oct 2015;36(10):928-30.
24 doi:10.1002/humu.22844
- 25 18. Rad A, Schade-Mann T, Gamerdinger P, *et al.* Aberrant COL11A1 splicing causes
26 prelingual autosomal dominant nonsyndromic hearing loss in the DFNA37 locus. *Hum Mutat.*
27 Jan 2021;42(1):25-30. doi:10.1002/humu.24136

- 1 19. Tompson SW, Young TL. Assaying the Effects of Splice Site Variants by Exon Trapping
2 in a Mammalian Cell Line. *Bio Protoc.* May 20 2017;7(10)doi:10.21769/BioProtoc.2281
- 3 20. LaFave MC, Varshney GK, Vemulapalli M, Mullikin JC, Burgess SM. A defined
4 zebrafish line for high-throughput genetics and genomics: NHGRI-1. *Genetics.* Sep
5 2014;198(1):167-70. doi:10.1534/genetics.114.166769
- 6 21. van de Beek MC, Dijkstra IM, Kemp S. Method for Measurement of Peroxisomal Very
7 Long-Chain Fatty Acid Beta-Oxidation and De Novo C26:0 Synthesis Activity in Living Cells
8 Using Stable-Isotope Labeled Docosanoic Acid. *Methods Mol Biol.* 2017;1595:45-54.
9 doi:10.1007/978-1-4939-6937-1_5
- 10 22. Kallemeijn WW, Lanyon-Hogg T, Panyain N, *et al.* Proteome-wide analysis of protein
11 lipidation using chemical probes: in-gel fluorescence visualization, identification and
12 quantification of N-myristoylation, N- and S-acylation, O-cholesterylation, S-farnesylation and
13 S-geranylgeranylation. *Nat Protoc.* Nov 2021;16(11):5083-5122. doi:10.1038/s41596-021-
14 00601-6
- 15 23. Kallemeijn WW, Lueg GA, Faronato M, *et al.* Validation and Invalidation of Chemical
16 Probes for the Human N-myristoyltransferases. *Cell Chem Biol.* Jun 20 2019;26(6):892-900 e4.
17 doi:10.1016/j.chembiol.2019.03.006
- 18 24. Perez-Riverol Y, Csordas A, Bai J, *et al.* The PRIDE database and related tools and
19 resources in 2019: improving support for quantification data. *Nucleic Acids Res.* Jan 8
20 2019;47(D1):D442-D450. doi:10.1093/nar/gky1106
- 21 25. Scott CA, Marsden AN, Slusarski DC. Automated, high-throughput, in vivo analysis of
22 visual function using the zebrafish. *Dev Dyn.* May 2016;245(5):605-13. doi:10.1002/dvdy.24398
- 23 26. Kurolap A, Kreuder F, Gonzaga-Jauregui C, *et al.* Bi-allelic variants in neuronal cell
24 adhesion molecule cause a neurodevelopmental disorder characterized by developmental delay,
25 hypotonia, neuropathy/spasticity. *Am J Hum Genet.* Mar 3 2022;109(3):518-532.
26 doi:10.1016/j.ajhg.2022.01.004
- 27 27. Eimon PM, Ghannad-Rezaie M, De Rienzo G, *et al.* Brain activity patterns in high-
28 throughput electrophysiology screen predict both drug efficacies and side effects. *Nat Commun.*
29 Jan 15 2018;9(1):219. doi:10.1038/s41467-017-02404-4

- 1 28. Rea V, Van Raay TJ. Using Zebrafish to Model Autism Spectrum Disorder: A
2 Comparison of ASD Risk Genes Between Zebrafish and Their Mammalian Counterparts. *Front*
3 *Mol Neurosci.* 2020;13:575575. doi:10.3389/fnmol.2020.575575
- 4 29. Basnet RM, Zizioli D, Taweedet S, Finazzi D, Memo M. Zebrafish Larvae as a
5 Behavioral Model in Neuropharmacology. *Biomedicines.* Mar 26
6 2019;7(1)doi:10.3390/biomedicines7010023
- 7 30. Bertencello KT, Bonan CD. Zebrafish as a tool for the discovery of anticonvulsant
8 compounds from botanical constituents. *Eur J Pharmacol.* Oct 5 2021;908:174342.
9 doi:10.1016/j.ejphar.2021.174342
- 10 31. Conant D, Hsiao T, Rossi N, *et al.* Inference of CRISPR Edits from Sanger Trace Data.
11 *CRISPR J.* Feb 2022;5(1):123-130. doi:10.1089/crispr.2021.0113
- 12 32. Ziermann JM, Diogo R. Cranial muscle development in frogs with different
13 developmental modes: direct development versus biphasic development. *J Morphol.* Apr
14 2014;275(4):398-413. doi:10.1002/jmor.20223
- 15 33. Berger J, Dorninger F, Forss-Petter S, Kunze M. Peroxisomes in brain development and
16 function. *Biochim Biophys Acta.* May 2016;1863(5):934-55. doi:10.1016/j.bbamcr.2015.12.005
- 17 34. Soupene E, Serikov V, Kuypers FA. Characterization of an acyl-coenzyme A binding
18 protein predominantly expressed in human primitive progenitor cells. *J Lipid Res.* May
19 2008;49(5):1103-12. doi:10.1194/jlr.M800007-JLR200
- 20 35. Mousnier A, Bell AS, Swieboda DP, *et al.* Fragment-derived inhibitors of human N-
21 myristoyltransferase block capsid assembly and replication of the common cold virus. *Nat Chem.*
22 Jun 2018;10(6):599-606. doi:10.1038/s41557-018-0039-2
- 23 36. Mainka T, Balint B, Govert F, *et al.* The spectrum of involuntary vocalizations in
24 humans: A video atlas. *Mov Disord.* Dec 2019;34(12):1774-1791. doi:10.1002/mds.27855
- 25 37. Singh S, Mishra SC, Israrahmed A, Lal H. Typical MRI features of PLA2G6 mutation-
26 related phospholipase-associated neurodegeneration (PLAN)/infantile neuroaxonal dystrophy
27 (INAD). *BMJ Case Rep.* Mar 25 2021;14(3)doi:10.1136/bcr-2021-242586

- 1 38. Franco G, Lazzeri G, Di Fonzo A. Parkinsonism and ataxia. *J Neurol Sci.* Feb 15
2 2022;433:120020. doi:10.1016/j.jns.2021.120020
- 3 39. Morales-Briceno H, Fung VSC, Bhatia KP, Balint B. Parkinsonism and dystonia: Clinical
4 spectrum and diagnostic clues. *J Neurol Sci.* Feb 15 2022;433:120016.
5 doi:10.1016/j.jns.2021.120016
- 6 40. Rossi M, Balint B, Millar Vernetti P, Bhatia KP, Merello M. Genetic Dystonia-ataxia
7 Syndromes: Clinical Spectrum, Diagnostic Approach, and Treatment Options. *Mov Disord Clin*
8 *Pract.* Jul-Aug 2018;5(4):373-382. doi:10.1002/mdc3.12635
- 9 41. Synofzik M, Schule R. Overcoming the divide between ataxias and spastic paraplegias:
10 Shared phenotypes, genes, and pathways. *Mov Disord.* Mar 2017;32(3):332-345.
11 doi:10.1002/mds.26944
- 12 42. Schor NF, Bianchi DW. Neurodevelopmental Clues to Neurodegeneration. *Pediatr*
13 *Neurol.* Oct 2021;123:67-76. doi:10.1016/j.pediatrneurol.2021.07.012
- 14 43. Deneubourg C, Ramm M, Smith LJ, *et al.* The spectrum of neurodevelopmental,
15 neuromuscular and neurodegenerative disorders due to defective autophagy. *Autophagy.* Mar 4
16 2022;18(3):496-517. doi:10.1080/15548627.2021.1943177
- 17 44. Leuzzi V, Nardecchia F, Pons R, Galosi S. Parkinsonism in children: Clinical
18 classification and etiological spectrum. *Parkinsonism Relat D.* Jan 2021;82:150-157.
19 doi:10.1016/j.parkreldis.2020.10.002
- 20 45. Sakai C, Ijaz S, Hoffman EJ. Zebrafish Models of Neurodevelopmental Disorders: Past,
21 Present, and Future. *Front Mol Neurosci.* 2018;11:294. doi:10.3389/fnmol.2018.00294
- 22 46. Varshney GK, Sood R, Burgess SM. Understanding and Editing the Zebrafish Genome.
23 *Adv Genet.* 2015;92:1-52. doi:10.1016/bs.adgen.2015.09.002
- 24 47. Hellsten U, Harland RM, Gilchrist MJ, *et al.* The genome of the Western clawed frog
25 *Xenopus tropicalis.* *Science.* Apr 30 2010;328(5978):633-6. doi:10.1126/science.1183670
- 26 48. De Robertis EM, Gurdon JB. A Brief History of *Xenopus* in Biology. *Cold Spring Harb*
27 *Protoc.* Dec 1 2021;2021(12)doi:10.1101/pdb.top107615

- 1 49. Nakayama T, Blitz IL, Fish MB, *et al.* Cas9-based genome editing in *Xenopus tropicalis*.
2 *Methods Enzymol.* 2014;546:355-75. doi:10.1016/B978-0-12-801185-0.00017-9
- 3 50. Ismail V, Zachariassen LG, Godwin A, *et al.* Identification and functional evaluation of
4 GRIA1 missense and truncation variants in individuals with ID: An emerging
5 neurodevelopmental syndrome. *Am J Hum Genet.* Jul 7 2022;109(7):1217-1241.
6 doi:10.1016/j.ajhg.2022.05.009
- 7 51. Naert T, Van Nieuwenhuysen T, Vleminckx K. TALENs and CRISPR/Cas9 fuel
8 genetically engineered clinically relevant *Xenopus tropicalis* tumor models. *Genesis.* Jan
9 2017;55(1-2)doi:10.1002/dvg.23005
- 10 52. Barbosa S, Greville-Heygate S, Bonnet M, *et al.* Opposite Modulation of RAC1 by
11 Mutations in TRIO Is Associated with Distinct, Domain-Specific Neurodevelopmental
12 Disorders. *Am J Hum Genet.* Mar 5 2020;106(3):338-355. doi:10.1016/j.ajhg.2020.01.018
- 13 53. Macken WL, Godwin A, Wheway G, *et al.* Biallelic variants in COPB1 cause a novel,
14 severe intellectual disability syndrome with cataracts and variable microcephaly. *Genome Med.*
15 Feb 25 2021;13(1):34. doi:10.1186/s13073-021-00850-w
- 16 54. Willsey HR, Exner CRT, Xu Y, *et al.* Parallel in vivo analysis of large-effect autism
17 genes implicates cortical neurogenesis and estrogen in risk and resilience. *Neuron.* Mar 3
18 2021;109(5):788-804 e8. doi:10.1016/j.neuron.2021.01.002
- 19 55. Nakayama T, Fisher M, Nakajima K, *et al.* *Xenopus pax6* mutants affect eye
20 development and other organ systems, and have phenotypic similarities to human aniridia
21 patients. *Dev Biol.* Dec 15 2015;408(2):328-44. doi:10.1016/j.ydbio.2015.02.012
- 22 56. Swierczynski SL, Siddhanti SR, Tuttle JS, Blackshear PJ. Nonmyristoylated MARCKS
23 complements some but not all of the developmental defects associated with MARCKS
24 deficiency in mice. *Dev Biol.* Oct 10 1996;179(1):135-47. doi:10.1006/dbio.1996.0246
- 25 57. Iioka H, Ueno N, Kinoshita N. Essential role of MARCKS in cortical actin dynamics
26 during gastrulation movements. *J Cell Biol.* Jan 19 2004;164(2):169-74.
27 doi:10.1083/jcb.200310027

28

1 **Figure legends**

2 **Figure 1 Family pedigrees, schematic variants' representation, conserved regions of**
 3 **substitution variants in *ACBD6*, and splicing effects. (A)** Pedigrees and segregation results for
 4 the 28 unrelated families. Double lines between individuals represent consanguinity. The 45
 5 affected individuals recruited for the study are shaded and indicated with their respective subject
 6 (S) number (S1, S2 or S3). The segregation data for all individuals tested via Sanger sequencing is
 7 shown with the presence of the *ACBD6* variant (red) and/or the reference allele (black), two
 8 red/black texts indicate a homozygous state, and one red + one black text indicates a heterozygous
 9 state. The genotyping is based on the coding DNA sequence. WT refers to wild type, DEL refers
 10 to deletion and DUP refers to duplication. **(B)** Schematic representation of the gene and protein
 11 positions of detected variants in *ACBD6*. *ACBD6* is located on chromosome 1 at cytogenetic
 12 position q25.2q25.3 (upper panel). The middle panel shows the genetic variants mapped to the
 13 NM_032360.4 transcript of *ACBD6*. The lower panel shows *ACBD6* variants mapped on the
 14 protein level. Three variants including p.(Gly22fs), p.(Leu121ThrfsTer27), and a 30kb deletion in
 15 the C-terminus have been reported previously.^{6, 7,10} Recurrent variants are labelled by family
 16 codes. **(C)** Splicing schematic for the c.574-2A>G variant in *ACBD6* showing cryptic acceptor
 17 splice site activation in exon 6 (upper panel). The c.664-2A>G (middle panel) and c.694+1G>A
 18 (lower panel) variants affect splicing of exon 7 both show exon skipping. Additionally, the
 19 c.694+1G>A variant activates a cryptic donor splice site. **(D)** Interspecies alignment performed
 20 with Clustal Omega showing the complete conservation down to invertebrates of the amino acid
 21 residues affected by a missense variant leading to an amino acid substitution p.(Asp201Gly) and
 22 an in-frame duplication p.(Asn219dup).

23
 24 **Figure 2 Clinical features of the affected individuals with bi-allelic *ACBD6* variants. (A) i-**
 25 **xiii:** Representative photographs demonstrating facial features of the affected individuals in
 26 adulthood. F1:S1 (i), F1:S2 (ii), F1:S3 (iii), F3:S2 (iv), F3:S1 (v), F6:S1 (vi), F7:S2 (vii), F7:S1
 27 (viii), F11:S1 (ix), F17:S1 (x), F17:S2 (xi), F20:S1 (xii), F16:S1 (xiii). xiv-xxxi: Representative
 28 photographs demonstrating facial features of the affected individuals in childhood. F3:S2 (xiv) at
 29 5 years old, F3:S1 (xv) at 12 years old, F6:S2 (xvi), F8:S1 (xvii), F8:S2 (xviii), F10:S1 (xix),
 30 F10:S2 (xx), and F11:S1 (xxi) at younger age, F13:S1 (xxii), F14:S1 (xxiii), F15:S1 (xxiv),

1 F16:S1 (xxv) at 2 years old, F16:S1(xxvi) at 4 years old, F19:S1 (xxvii), F19:S2 (xxviii), F20:S2
 2 (xxix), F12:S1 (xxx), F12:S2 (xxxi). The most frequently seen facial dysmorphologies in adults
 3 are high nasal ridge, full nasal tip, small mouth, thin upper lip, and broad chin. The most
 4 frequently seen facial dysmorphologies in children are bi-frontal/bi-temporal narrowing, arched
 5 eyebrows, hypertelorism, up-slanting palpebral fissures, depressed nasal bridge, full nasal tip,
 6 thin upper lip, full lower lip, and broad chin. **(B)** Representative photographs demonstrating
 7 postural abnormalities seen in the affected individuals. A stooped body posture and lateral
 8 flexion of the trunk can be seen in the individuals including F1:S1 (i), F1:S2 (ii), F1:S3 (iii),
 9 F3:S1 (iv), F3:S2 (v), F6:S1 (vi), F6:S2 (vii), and F8:S2 (viii), F13:S1 (ix). **(C)** Bar graph
 10 summarizing proportions of various clinical findings in the *ACBD6* cohort. Blue – affected,
 11 orange – unaffected, grey – not ascertained/not applicable. GDD, Global developmental delay.
 12 ID, Intellectual disability. **(D)** Representative neuroimaging features of the affected individuals.
 13 Brain MRI, midline sagittal images of the affected individuals F1:S1 (i), F1:S2 (ii), F5:S1(iii),
 14 F56:S2 (iv), F7:S1 (v), F7:S2 (vi), F10:S1 (vii), F10:S2 (viii), F11:S1 (ix), F13:S1 (x), F14:S1
 15 (xi), and F19:S1 (xii). Most of the affected individuals have corpus callosum agenesis or
 16 hypoplasia with prevalent involvement of the posterior sections (empty arrows), variably
 17 associated with short midbrain (thin arrows) and small inferior cerebellar vermis (arrowheads).
 18 In addition, mild hypertrophy of the clava was noted in some subjects (dotted arrows). Note that
 19 the anterior commissure was markedly hypoplastic or absent in all affected individuals.

20
 21 **Figure 3 CRISPR/Cas9 mutation of zebrafish *acbd6* causes smaller eyes, impaired vision,**
 22 **abnormal locomotion, developmental delay, and increased mortality. (A)** Whole-mount *in*
 23 *situ* hybridization for detecting *acbd6* mRNA expression pattern in zebrafish embryo at 24 hpf.
 24 Forebrain (fb), midbrain (mb), midbrain and hindbrain boundary (MHB), hindbrain (hb), otic
 25 vesicle (ov). Dorsal view, anterior to the left. **(B)** Representative images of wild-type
 26 (*acbd6*+/+), heterozygous (*acbd6*+/-) and homozygous (*acbd6*-/-) mutant larva at 6 dpf. Head
 27 size and eye size are indicated by blue and red lines, respectively. Anterior to the left and dorsal
 28 to the top. Scale bar = 200 μ m. **(C, D)** Quantification of eye and head size as indicated in Fig.
 29 3B. +/+ (n = 26 larvae), +/- (n = 114 larvae) and -/- (n = 47 larvae). Each symbol represents one
 30 larva. Values are calculated as a percentage of the mean value of +/+ larvae. Error bars = mean \pm

1 standard deviation (SD). **(E)** The result of VSR analysis performed on $+/+$ ($n = 43$ larvae), $+/-$ (n
2 $= 99$ larvae), and $-/-$ ($n = 48$ larvae) zebrafish larvae at 6 dpf. Each symbol represents one larva.
3 The number of responses for 5 stimuli of each larva is calculated as a percentage of responses.
4 Error bars = mean \pm standard error of the mean (SEM). **(F)** Locomotor activities of zebrafish
5 larvae in light and dark periods at 6 dpf. $+/+$ ($n = 42$ larvae), $+/-$ ($n = 99$ larvae), and $-/-$ ($n = 48$
6 larvae) zebrafish larvae were habituated in the dark for 30 minutes, followed by three cycles of
7 10-minute time bins of light and dark periods. Error bars = mean \pm SEM. The dark period (D)
8 and light period (L) are labelled. Black arrows indicate the increased movement of homozygous
9 mutants at the first minute in the dark. **(G)** Average cumulative distance traveled of each larva
10 from three cycles of either light or dark periods in Fig. 3F. Error bars = mean \pm SD. **(H)** Average
11 cumulative distance traveled of each larva during the first minute of the dark period across three
12 cycles as indicated by black arrows in Fig. 3F. Error bars = mean \pm SD. **(I)** Locomotor activities
13 of zebrafish larvae in light and dark conditions at 12 dpf. $+/+$ ($n = 39$ larvae), $+/-$ ($n = 71$ larvae)
14 and $-/-$ ($n = 29$ larvae). Error bars = mean \pm SEM. Red arrow indicates increased movement of
15 homozygous mutants at the first minute after light on. Red arrowhead indicates increased
16 movement of homozygous mutants at the second minute after light on. **(J)** Average cumulative
17 distance traveled by each larva during three cycles of either light or dark periods in Fig. 3I. Error
18 bars = mean \pm SD. **(K)** Average cumulative distance traveled by each larva during the first cycle
19 of the first minute of the light period as indicated by red arrow in Fig. 3I. Error bars = mean \pm
20 SD. **(L)** Genotyping results of zebrafish at 6 dpf ($n = 191$ larvae), 12 dpf ($n = 196$ larvae) and 30
21 dpf ($n = 118$ juveniles) stages from *acbd6* $+/+$ intercross. **(M)** Representative images of
22 morphological phenotype from *acbd6* $+/+$, *acbd6* $+/-$ and *acbd6* $-/-$ at 30 dpf. Anterior to the left
23 and dorsal to the top. **(N)** Sagittal section of *acbd6* $+/+$ brain at 30 dpf. Anterior to the left and
24 dorsal to the top. Olfactory bulb (Ob), periventricular gray zone of optic tectum (PGZ), medulla
25 oblongata (MO). **(O-W)** Representative images of transverse sections of telencephalon (O-Q),
26 optic tectum (R-T) and cerebellum (U-W) from *acbd6* $+/+$, *acbd6* $+/-$ and *acbd6* $-/-$ juvenile as
27 indicated in Fig. 3N. In (C, D), one-way ANOVA with Tukey's multiple comparisons test. In (E,
28 G, H, J, K), one-way ANOVA with Dunnett's T3 multiple comparisons test. ns, not significant p
29 ≥ 0.05 , $*p < 0.05$, $**p < 0.01$, $***p < 0.001$ and $****p < 0.0001$.

30

1 **Figure 4 Zebrafish *acbd6* F₀ knockouts exhibit increased susceptibility to chemical-induced**
2 **seizures, excessive motor neuron branching, and skeletal muscle degeneration. (A)**
3 Representative images of uninjected control and *acbd6* F₀ larvae at 6 dpf. Left column, ventral
4 view, anterior to the left. Right column, dorsal view, anterior to the left. Blue line indicates head
5 size, magenta line indicates eye size, and cyan line indicates eye distance. Scale bar = 0.2 mm.
6 **(B, C)** Quantification of the head and eye size (n = 30 larvae for each group) of uninjected
7 control (uninj.), *acbd6* F₀ knockout (F₀), F₀ + zebrafish wild-type *acbd6* mRNA (+*acbd6*), and F₀
8 + human wild-type *ACBD6* mRNA (+*ACBD6*) as indicate in Fig. 4B. **(D)** The VSR analysis
9 after mRNA rescue at 6 dpf. n = 36 larvae for each group. Each symbol represents one larva. The
10 number of responses to 5 stimuli of each larva was calculated as a percentage of responses. Error
11 bars = mean ± SEM. **(E)** Quantification of the eyes distance (n = 20 larvae for each group) as
12 indicate in Fig. 4B. **(F)** Quantification of the eye size of F₀ knockout rescued with mRNA of
13 human p.Glu63Ter (+E63*) or p.Asp201Gly (+D201G) variant. n = 25 larvae for each group.
14 **(G)** Locomotor activities of zebrafish larvae in light and dark conditions at 6 dpf. n = 64 larvae
15 for each group. The larvae were habituated in the dark for 30 minutes, followed by three cycles
16 of 10-minute periods of light and dark. Error bars represent the mean ± SEM. Dark period (D),
17 light period (L). Red arrows indicating increased movement of F₀ one minute after light on, and
18 black arrows indicate increased movement one minute after light off. **(H)** Average cumulative
19 distance traveled by each larva during three cycles of either light or dark periods in Fig. 4G.
20 Error bars = mean ± SD. **(I)** The average cumulative distance traveled by each larva during the
21 first minute of the dark period was measured over three cycles, as shown by the black arrow in
22 Fig. 4G. Error bars represent the mean ± SD. **(J)** The average cumulative distance traveled by the
23 larvae was measured for each group after being treated with different doses of pentylenetetrazole
24 (PTZ) at 5 dpf. n = 16 larvae for each group. **(K-N)** Confocal images of
25 *Tg(mnx1:GFP;olig2:DsRed)* larva at 12 dpf are shown, with transgenic larvae injected with
26 *slc45a2* sgRNA used as a control and those injected with *acbd6* + *slc45a2* sgRNAs shown as
27 *acbd6* F₀. (L' and N') Enlarged images from white boxes are shown in L' and N', with red
28 asterisks indicating autofluorescence from remaining pigment cells. GFP and DsRed are
29 displayed in cyan and magenta, respectively, with magenta arrowheads indicating excess axonal
30 arborizations. The images are presented in a lateral view, with anterior to the left and dorsal to
31 the top. Additional motor neuron phenotypes at 6 and 12 dpf can be found in Supplementary Fig.

1 13. **(O-T)** Confocal images of stained skeletal muscle fibers with phalloidin are presented,
2 including images from *slc45a2* sgRNA-injected control (O-Q) and *acbd6* + *slc45a2* sgRNAs-
3 injected (R-S) larvae at 12 dpf. Orthogonal views generated from (P and S) using the Orthogonal
4 views tool in ImageJ are also displayed. Degenerated muscles are indicated by (#), while white
5 arrowheads and a white arrow indicate Z-discs and the thickness of the myotube, respectively.
6 Supplementary Fig. 14 provides additional muscle phenotypes at 6 and 12 dpf. In (B-D and F),
7 one-way ANOVA with Tukey's multiple comparisons test. In (E and H-J), one-way ANOVA
8 with Dunnett's T3 multiple comparisons test. ns, not significant $p \geq 0.05$, * $p < 0.05$, ** $p < 0.01$,
9 *** $p < 0.001$ and **** $p < 0.0001$.

10

11 **Figure 5 *acbd6* *X. tropicalis* crispants have gastrulation, movement, craniofacial, brain and**
12 **eye defects together with microcephaly. (A)** The gene structure of human (*ACBD6*) and *X*
13 *.tropicalis* (*acbd6*) reveals 8 exons. **(B)** Gastrulation defects, including failure of blastopore
14 closure and anterior posterior defects, were observed in F₀ *X. tropicalis* embryos injected with
15 two different CRISPR/Cas9 constructs (sgRNA-68 and sgRNA-71) disrupting exon 1 of *acbd6*.
16 **(C)** Those animals surviving to free-feeding stages presented with microcephaly, craniofacial
17 dysmorphism and eye abnormalities. **(D)** The differences in head size between the uninjected
18 control (2.07 +/- 0.36mm) and *acbd6* crispant tadpoles (1.52 +/- 0.27mm, sgRNA-68) were
19 found to be significant, $t(34)=5.183$, $p<0.001$. **(E-F)** Alcian Blue staining marking the
20 cartilaginous structures in the head and neck show equivalent structures between control **(E)** and
21 *acbd6* crispant tadpoles **(F)** revealing no gross morphological abnormalities. **(G)** Detailed
22 structural analysis in higher resolution MicroCT imaging (1% phosphotungstic acid contrast
23 stain) revealed significant structural abnormalities in the facial musculature (Red arrows, G),
24 abnormalities of the eye (microphthalmia, anophthalmia – Yellow arrows, G) and structural
25 abnormalities in the brain most pronounced in the midbrain regions (Blue arrow, G). **(H)**
26 Locomotion analysis at NF44/45 revealed that crispants moved significantly less than control
27 tadpoles. **(I)** The Kaplan-Meier survival analysis of 65 control and crispant tadpoles shows two
28 periods of crispant-specific decline, the first at gastrula stages (day 0-1) and the second with
29 post-feeding (day 8, NF stage 47).

30

1 **Figure 6 Morphological characteristics of peroxisomes in *ACBD6*-deficient patient cells are**
2 **not altered and chemical proteomic profiling of *N*-myristoylation in human fibroblasts. (A)**
3 Patient fibroblasts and controls were processed for immunofluorescence microscopy using
4 antibodies against the peroxisomal membrane marker PEX14, the matrix marker catalase, or
5 mitochondrial ATP synthetase B (ATPB). Peroxisomal localisation of PEX14 and catalase
6 indicate that peroxisomal membrane and PTS1-dependent matrix import are normal. Note that
7 the morphology of mitochondria, which are elongated in fibroblasts, was also not altered when
8 compared to controls. **(B)** Quantification of peroxisome number based on immunofluorescence
9 images (see A for representative images) ($n = 29$ -36 cells). Data are from three independent
10 experiments. ns, not significant; Kruskal-Wallis ANOVA test with Dunn's multiple
11 comparisons. **(C)** COS-7 cells were transfected with plasmids encoding Myc-ACBD5 or Myc-
12 ACBD6 and processed for immunofluorescence microscopy using antibodies against Myc and
13 PEX14. Note that Myc-ACBD5 localises to peroxisomes, whereas Myc-ACBD6 localises to the
14 nucleus and the cytoplasm in COS-7 cells. Scale bars, 10 μm . **(D)** Ranked plot of YnMyr-
15 labelled, known co- and post-translationally *N*-myristoylated proteins, as identified in
16 (Supplementary Figure 18E). Position on the left equals lower abundance in ACBD6 deficient
17 fibroblasts, position on the right equals higher abundance in ACBD6 deficient fibroblasts.

18
19 **Figure 7 Chemical and whole proteome analysis of *acbd6* wild-type and crisprant zebrafish**
20 **and *X. tropicalis* model systems. (A)** Volcano plot comparing YnMyr labelling of proteins in
21 wild-type and *acbd6* crisprant zebrafish at 72 hpf. Horizontal dotted line: significance threshold
22 (p -value = 0.05). FC: fold-change. Position on the left equals reduced in crisprant, position on the
23 right equals increased in crisprant. **(B)** Comparing YnMyr labelling of proteins in wild-type and
24 *acbd6* crisprant zebrafish at 120 hpf. Further description as in (A). **(C)** Top-20 of biological
25 processes most significantly enriched in proteins down-regulated in *acbd6* crisprant zebrafish at
26 72 hpf. The most significantly enriched process at the top. Colour indicates Q-value as secondary
27 significance indicator. Size of circles indicates a number of proteins enriched in the depicted
28 process. Dr: *Danio rerio*. Hs: *Homo sapiens*. **(D)** Volcano plot comparing YnMyr labelling of
29 proteins in wild-type and *acbd6* crisprant 68 *X. tropicalis*. Horizontal dotted line: significance
30 threshold (p -value = 0.05). FC: fold-change. Position on the left equals reduced in crisprant,
31 position on the right equals increased in crisprant. **(E)** Comparing YnMyr labelling of proteins in

1 wild-type and *acbd6* crisprant 71 *X. tropicalis*. Further description as in (D). (F) Top-20 of
2 biological processes most significantly enriched in proteins up-regulated in *acbd6* crisprant 68 *X.*
3 *tropicalis*. Most significantly enriched processes are at the top. Colour indicates Q-value as
4 secondary significance indicator. Size of circles indicates a number of proteins enriched in the
5 depicted process. Xt: *Xenopus tropicalis*. Hs: Homo sapiens.

6

7

8

ACCEPTED MANUSCRIPT

1 Table I Main clinical features of the affected individuals with homozygous ACBD6 variants

Family ID	1	2	3	4	5	6	7	8	9	10	11	12	13	14	15	16	17	18	19	20	21	22	23	24	25	26	27	28
N of affected	3	1	2	1	2	2	2	2	1	2	1	2	1	1	1	1	2	1	2	2	1	2	2	1	1	2	2	2
GDD/ID	3+	+	2+	+	2+	2+	2+	2+	+	2+	+	2+	+	+	+	+	2+	+	2+	2+	+	2+	2+	+	+	2+	2+	2+
Progressive disease course	3+	X	2+	X	2+	2+	2+	2+	X	2+	+	2X	+	+	+	X	2+	X	2X	2X	+	2X	2+	+	X	2X	2+	2+
Microcephaly	1+	-	2-	+	2-	1+	1+	2+	X	2-	-	2-	+	-	-	+	2X	-	2+	2X	-	2X	2-	+	X	2X	1+	2X
Short stature	3-	+	1+	X	2-	2+	2+	2+	-	2-	+	2-	+	+	-	X	2X	X	2-	2+	+	2X	1- = 1X	+	X	2X	2X	2X
Facial dysmorphism	3+	+	2+	X	2+	2+	2+	2+	+	2+	+	2+	+	+	+	+	2+	X	2+	2+	+	2X	2-	+	X	2X	2+	2+
Oculomotor abnormalities	3X	X	2+		2+	2+	2X	1+	X	2+	-	2+	+	-	+	+	2X	+	2-	1+	+	2X	2-	X	X	2X	2+	2X
Cerebellar ataxia	3+	+	1+	+	2+	2+	2+	2+	-	2+	+	2+	+	+	+	+	2+	X	2+	2+	-	2X	2-	-	X	2+	2+	2+
Limb spasticity/hypertonia	3+	+	2+	+	2+	1+	2+	2+	-	2+	-	2-	+/-	+	+/-	+	2+	X	2+	2-	-	2X	1+ = 1-	-	X	2+	2+	2+
Gait abnormalities	1+	+	2+	+	2+	2+	2+	2+	-	2+	+	2+	+	X	+	+	2+	+	2+	2X _p	X	2X	1+ = 1X	X	X	2+	2+	2+
No independent gait	1+	+	2-	X	2-	2-	2-	2-	-	1+	-	2-	-	+	-	-	1+	-	2+	2+	+	2X	1- = 1X	+	+	2X	2-	2-
Hypokinesia/Parkinsonism	3+	X	1+	X	2-	2+	2X	2-	X	2X	X	2-	-	-	-	+	1+	X	2-	2-	-	2X	2-	-	X	2X	1+	1+
Truncal/limb dystonia	3+	X	2+	X	2+	2+	2X	2+	X	2+	+	1+ = 1-	+	+	+	+	2+	X	2+	2+	+	2X	2X	-	X	2X	2+	2+
Upper limb/head tremor	3X	+	2+	+	2+	2+	2-	2-	-	2+	+	2-	+	+	+	+	2+	+	2+	2-	-	2X	2-	-	X	2X	2+	2X
Tics and TLV	1+	X	1+	X	2X	2X	2X	2+	X	2-	-	2X	+	X	X	X	2X	-	2X	1+	-	2X	2-	-	X	2X	1+	2X
Postural instability	2+	X	2-	X	2+	2X	2X	2+	X	2+	+	2-	+	+	+	+	2X	X	2X	2X	X	2X	1- = 1X	X	X	2X	2+	2+
Epileptic seizures	2+	+	2-	+	2+	2-	2-	2-	+	2-	-	2-	+	-	-	+	2X	-	2-	2-	+	2X	1+ = 1-	-	+	2X	2-	2-
Behavioural problem	3+	-	2-	-	2+	2+	2+	2-	-	2+	-	2-	+	+	+	+	2X	X	2+	2+	-	2X	1+ = 1-	-	X	2X	2+	2+
Premature aging	3+	-	2-	-	2-	1+	1+	2-	-	2-	-	2-	-	-	-	-	2+	-	2-	2-	-	2X	2-	-	X	2X	2-	2+
Reduction of PWM	2+ ^a	X	1+	X	1+	1+	1+	1- ^a	X	2+	-	2X	+	-	-	X	2X	X	2-	2-	X	2X	2X	X	X	2X	2-	2X
CC hypoplasia/agenesis	2+ ^a	+	1+	X	1+	1+	2+	1- ^a	X	2+	+	2X	-	+	-	+	2+	X	2+	2-	+	2X	2X	X	X	2X	2+	2X
AC Hypoplasia/agenesis	2+ ^a	X	2-	X	2+	2+	2+	1+ ^a	X	2+	+	2X	+	+	+	X	2X	X	2+	2-	X	2X	2X	X	X	2X	2+	2X
Short midbrain	2+ ^a	X	2-	X	1+	2+	1+	1+ ^a	X	2+	+	2X	-	+	-	X	2X	X	2-	2-	X	X	2X	X	X	2X	2-	2X

ICV hypoplasia	2 ⁺ ^a	X	2 ⁻	X	1 ⁺	2 ⁺	1 ⁺	1 ⁺ ^a	X	1 ⁺	-	2X	+	+	-	X	2X	X	2 ⁻	2 ⁻	+	2X	2X	X	X	2X	2 ⁻	2X
Hypertrophy of the clava	2 ⁻ ^a	X	2 ⁻	X	2 ⁻	1 ⁺	1 ⁻	1 ⁻ ^a	X	2 ⁻	-	2X	+	+	-	X	2X	X	2 ⁺	2 ⁻	X	2X	2X	X	X	2X	2 ⁻	2X

- 1 - = negative for the feature of interest; + = positive for the feature of interest; +/- = mild hypertonia; AC = anterior commissure; CC = corpus callosum; F = family; GDD = global developmental delay; ICV = hypoplasia of the inferior cerebellar vermis; ID = intellectual disability; N = number; PWM = periventricular white matter; TLV = tic like vocalizations; X = not available/not applicable.
- 2 The numbers preceding the symbols "+", "-", and "X" indicate the number of siblings who are positive, negative or don't have data on the feature of interest in families with multiple affected.
- 3 ^aBrain MRI scans are not available from another affected sibling.
- 4
- 5

ACCEPTED MANUSCRIPT

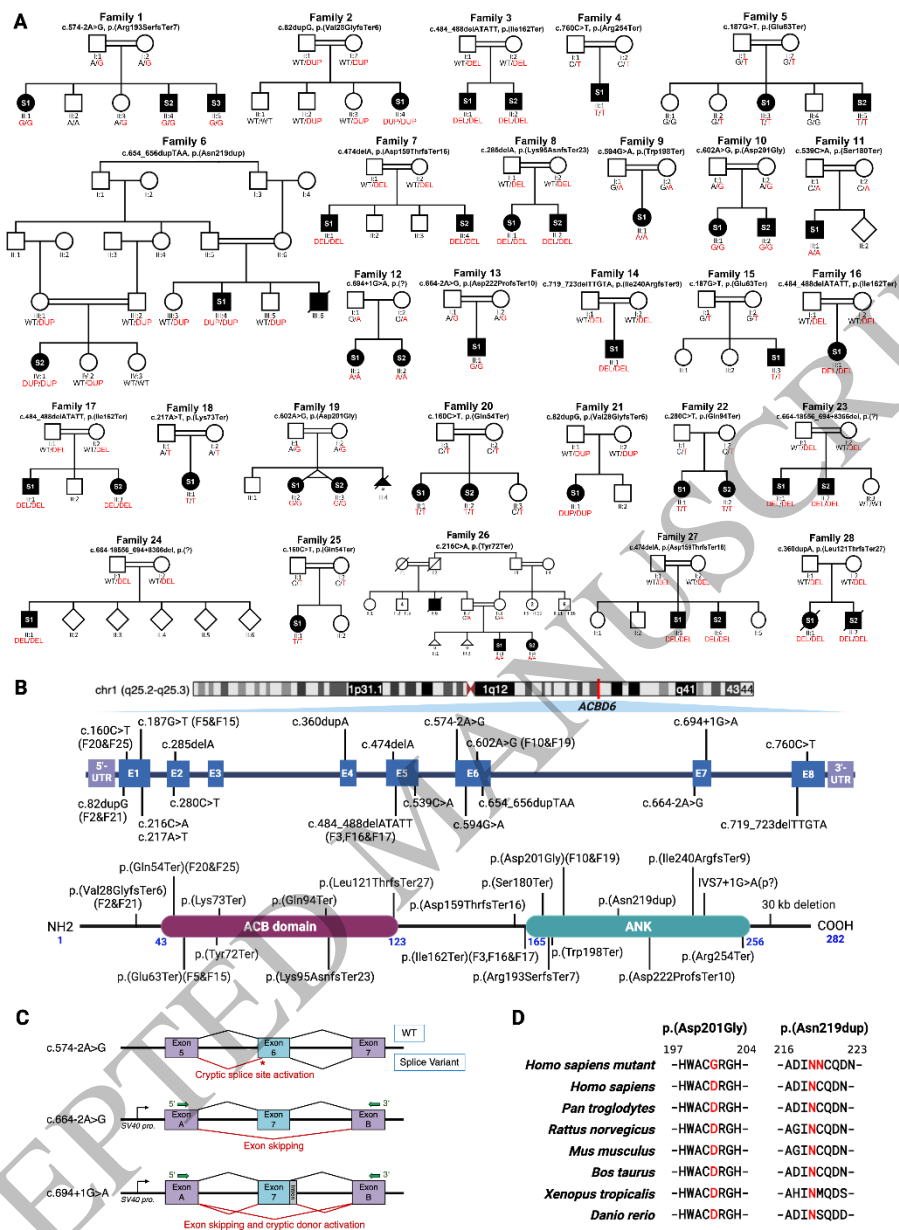


Figure 1
246x336 mm (x DPI)

1
2
3
4

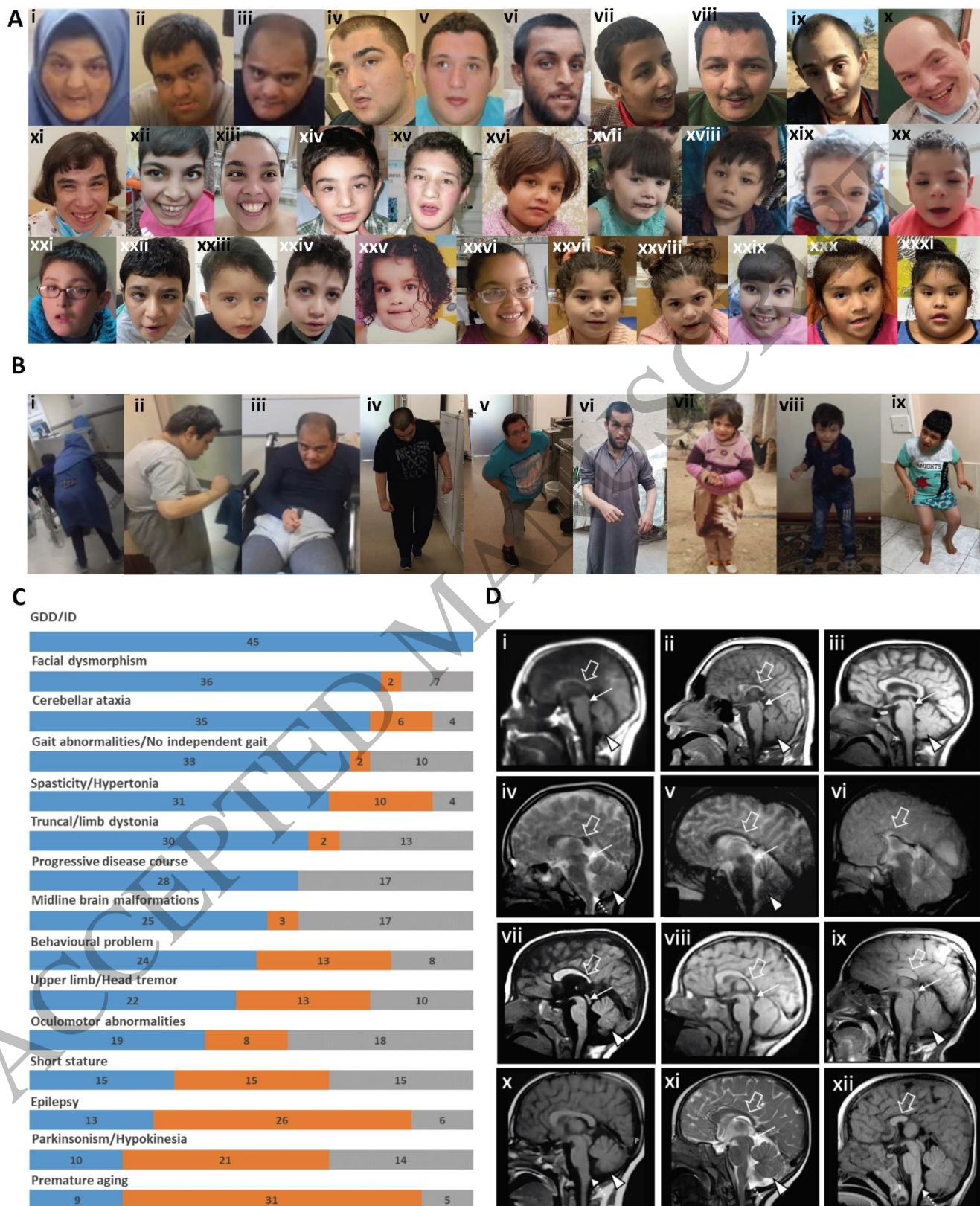


Figure 2
185x230 mm (x DPI)

1
2
3

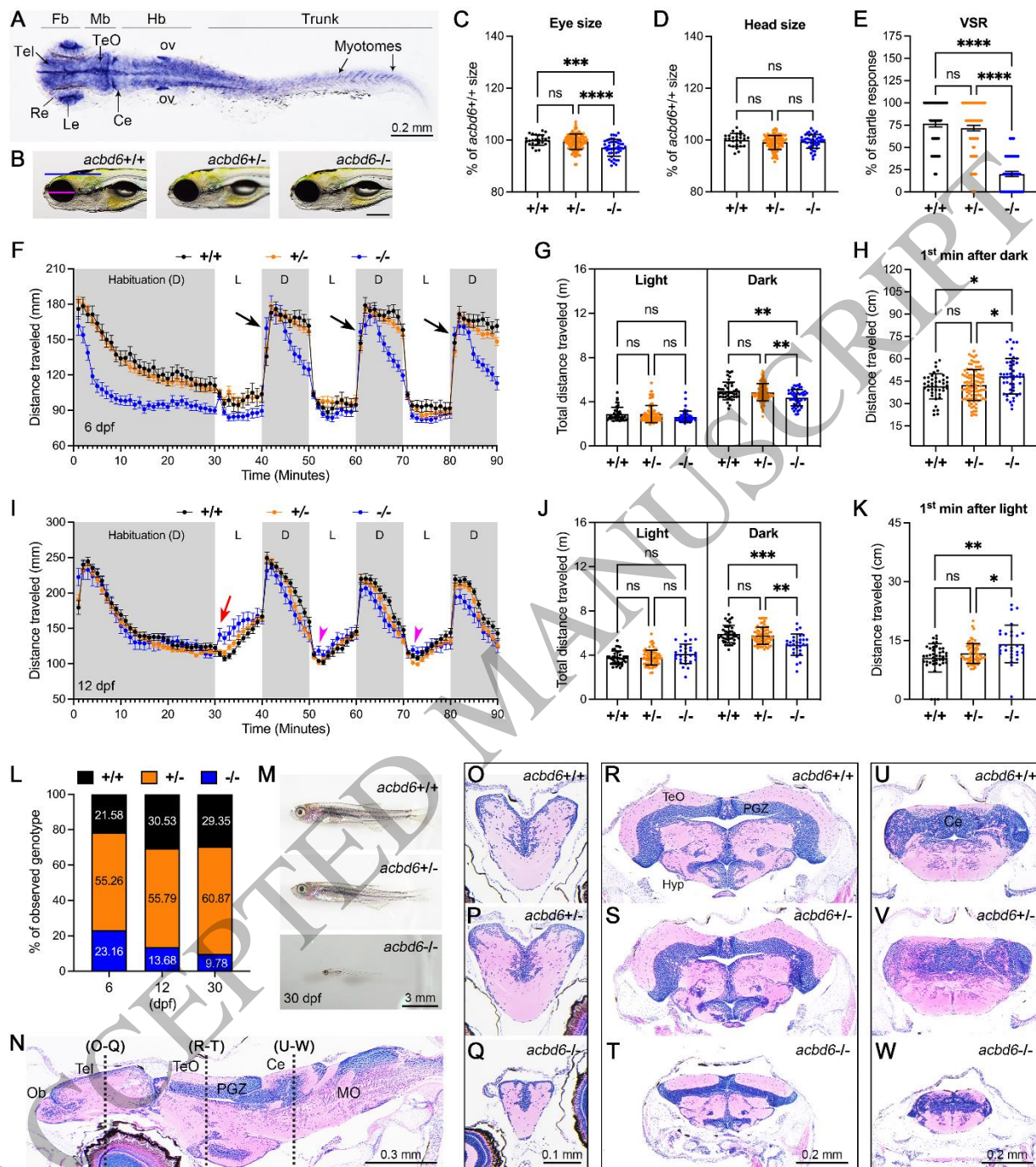


Figure 3
305x344 mm (x DPI)

1
2
3
4

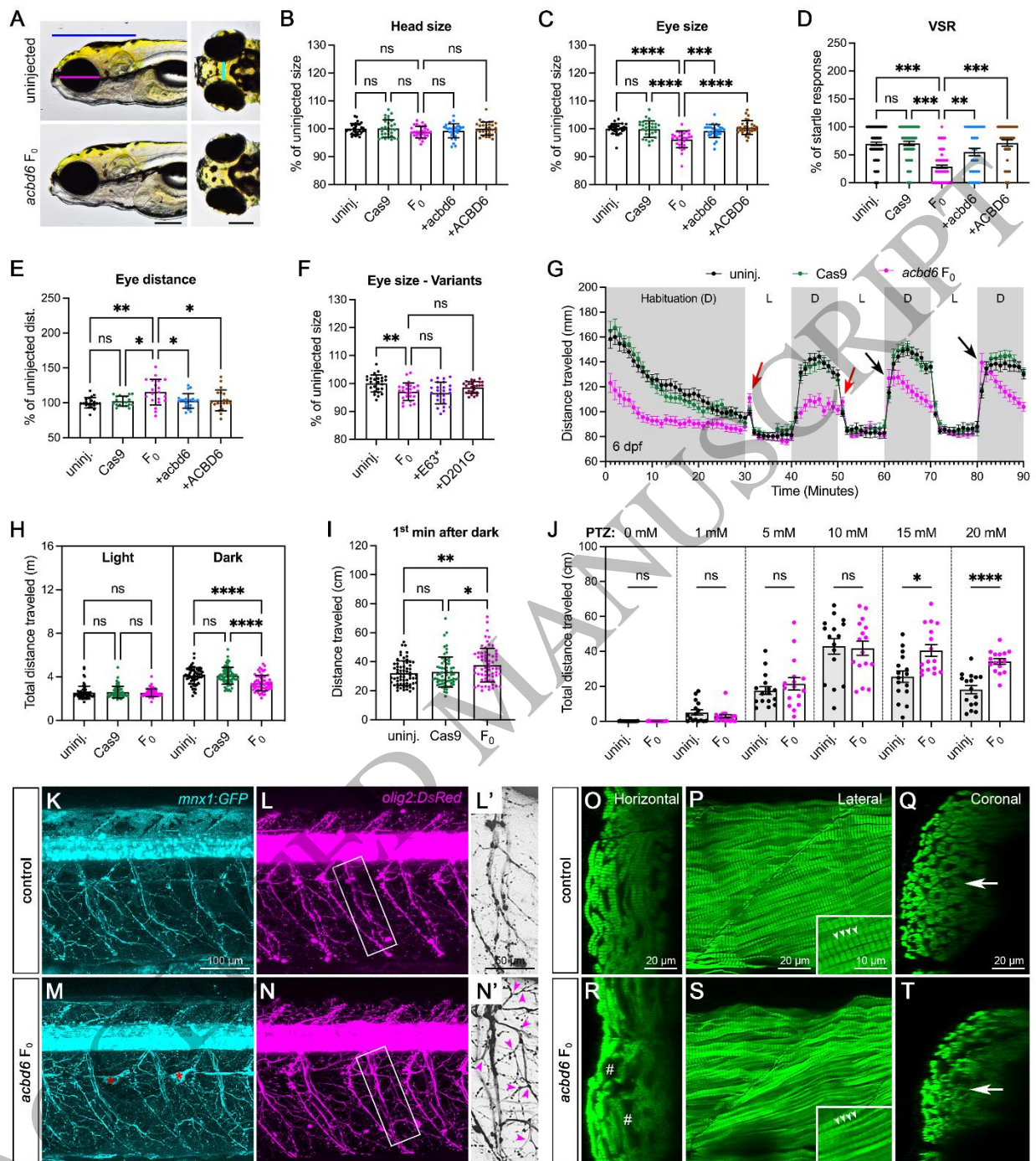
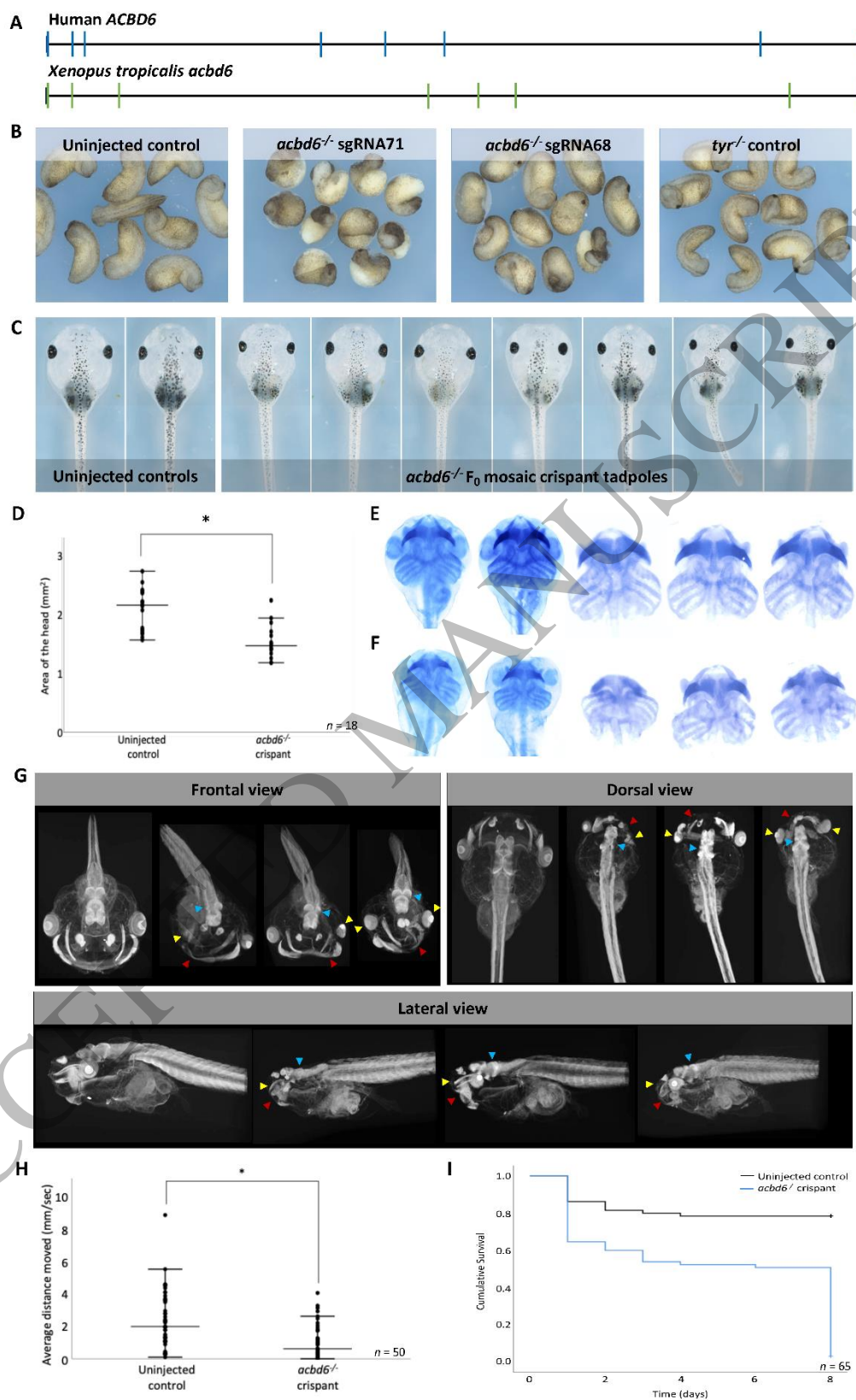


Figure 4
 305x345 mm (x DPI)

1
 2
 3
 4



1
 2
 3

Figure 5
 176x275 mm (x DPI)

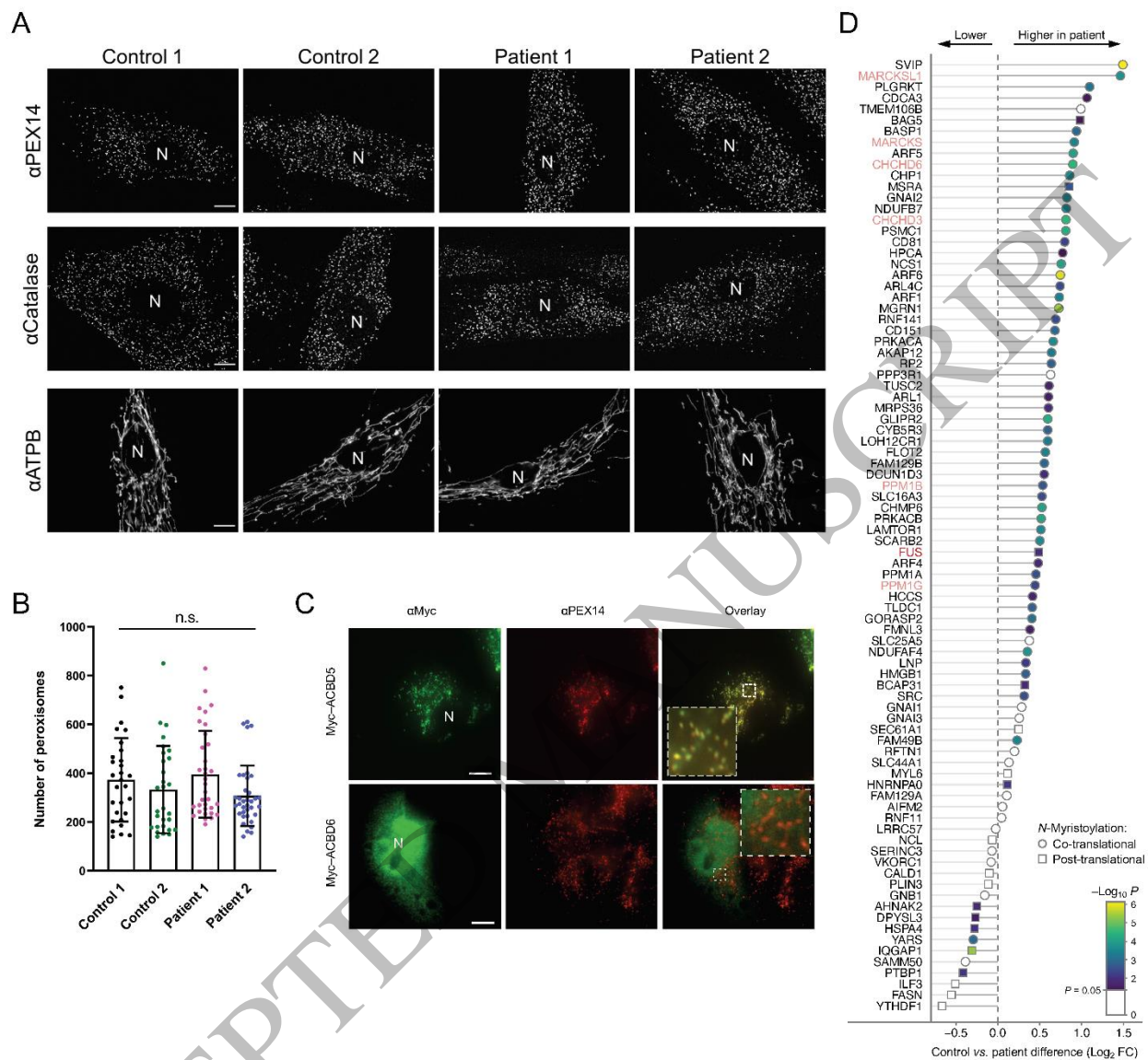
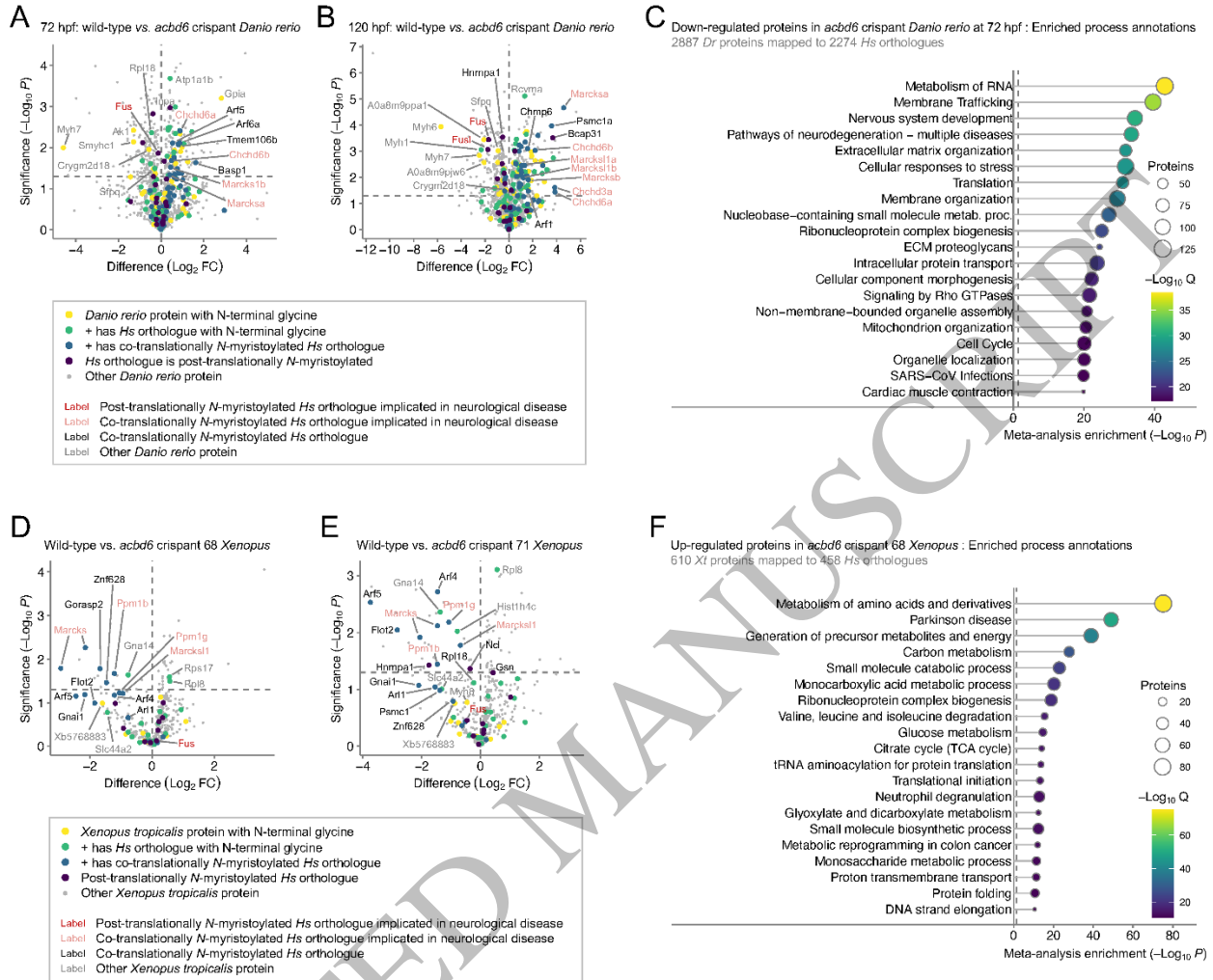


Figure 6
 339x316 mm (x DPI)

1
 2
 3
 4
 5



1
2
3

Figure 7
339x283 mm (x DPI)